Optical Time Division Multiplexing Scheme Using Soliton Interaction

OPTICAL TIME DIVISION MULTIPLEXING SCHEME USING SOLITON INTERACTION

By

PENGJU ZHANG

B. Eng., Xidian University (2002)

A Thesis

Submitted to the School of Graduate Studies

in Partial Fulfilment of the Requirements

for the Degree

Master of Applied Science

MCMASTER UNIVERSITY

Master of Applied Science (2006)   McMaster University

Electrical and Computer Engineering   Hamilton, Ontario

TITLE   Optical Time Division Multiplexing Scheme Using Soliton Interaction

AUTHOR   Pengju Zhang,   B. Eng. (Xidian University)

SUPERVISOR   Dr. Shiva Kumar

PAGES   50

Abstract

An optical time division multiplexing (TDM) scheme using soliton interaction is proposed in the thesis to save the time-bandwidth prduct (TBP). The soliton multiplexer (MUX) consisting of a highly nonlinear fiber (HNLF) combines two adjacent solitons to form a composite soliton, while the soliton demultiplexer (DEMUX) consisting of a similar HNLF restores the component solitons. The case of interaction between identical fundamental solitons is discussed first. However, when this scheme is used in the conventional TDM system, the total bit rate transmitted over the channel is limited by the time interval between the two adjacent component solitons. Therefore, a modified multiplexing scheme using interaction between different solitons is proposed to satisfy more practical engineering applications. The theoretical analysis and numerical simulation results demonstrate that the modified optical TDM scheme offers a higher TBP efficiency and suitable for conventional TDM, which makes it an attractive candidate for meeting the challenge of increasing demand on frequency bandwidth in modern optical communications.

Acknowledgements

I would like to express my sincere gratitude to Dr. Shiva Kumar, for both leading me to this interesting field, and making sure that I was going forward in the right direction. Through his roles as a supervisor and a mentor, Dr. Kumar has had a tremendous impact on both my professional and personal development.

For his guidance and encouragement, I also wish to thank Dr. Weiping Huang. His courses and seminars have greatly influenced the way I think about research problems. I am sincerely grateful to Ms. Rong Chai for her many insightful comments, her encouragement and her numerous discussions relating to this work.

The friendly atmosphere and productive research environment of the Photonics Group have made my experiences as a graduate student both challenging and rewarding. Thanks to Ling Liu, Dong Yang and Xianming Zhu for their help with various parts of the thesis and thought-provoking discussion.

I am especially grateful to Cosmin Coroiu for his computer expertise and friendship. Special thanks go to Cheryl Gies and Helen Jachna for administrative support and for help in preparing this thesis.

Finally, I would like to thank my grandparents, parents and sister for their unending love, understanding and encouragement.

Contents

List of Figures

List of Tables

List of Abbreviations

ASE	Amplified Spontaneous Emission
AWGN	Additive White Gaussian Noise
BER	Bit Error Rate
CW	Continuous Wave
DEMUX	Demultiplexer
EAM	Electro-Absorption Modulator
FDM	Frequency Division Multiplexing
FPGA	Field Programmable Gate Array
FWHM	Full Width at Half Maximum
GVD	Group Velocity Dispersion
HNLF	Highly NonLinear Fiber
ISI	Inter-Symbol Interference
IST	Inverse Scattering Transform
KdV	Korteweg-de Vries equation
MUX	Multiplexer
NSE	Nonlinear Schrödinger Equation
OOK	On-Off Keying
PSD	Power Spectral Density
RMS	Root Mean Square
SNR	Signal to Noise Ratio
SPM	Self-Phase Modulation
TBP	Time-Bandwidth Product

TDM   Time Division Multiplexing

WDM   Wavelength Division Multiplexing

Chapter 1

Introduction

1.1   Motivation and Methodology

Time-bandwidth product (TBP) of a signal is an important parameter for time division multiplexing (TDM) as well as wavelength division multiplexing (WDM) systems. The reduction in temporal width enables to multiplex more channels in TDM systems, while reduction in bandwidth enables to multiplex more channels in WDM systems. As the temporal width decreases, the bandwidth increases. Therefore, to multiplex more channels in a TDM system to reach a certain total bit rate, one needs to choose the signal that occupies the minimum frequency bandwidth.

When two identical optical solitons are sufficiently close by, the nonlinear interaction leads to attractive or repulsive force between them depending on the relative phase difference between them being 0 or π. If the phase difference is 0, the force is attractive, and the solitons collide to form a composite soliton. A soliton multiplexing scheme using Toda solitons in electrical communication systems is originally proposed by A. C. Singer, *et. al.* [1] for energy minimization, and also by R. Chai and K. M. Wong [2] for the time-bandwidth product (TBP) minimization. In this thesis, we implement the concept of TBP in [2] in optical domain using the nonlinear Schrödinger soliton. The differences between the implementation in electrical and optical domains are

1. the channel is quasi-linear for fiber optical transmission systems, and

2. the receiver is incoherent since the photo detector is a square-law device.

1.2   Outline of the Thesis

There are a lot of literatures on soliton theory spanning over the past century of research. Rather than providing a self-contained summary, in Chap.2 we give a brief overview of the soliton theory, with special concentration on fiber solitons described by the well-known nonlinear Schrödinger equation (NSE), which we will draw upon throughout the thesis.

To facilitate real-time processing of soliton signals, it is important to explore implementations of the corresponding nonlinear systems. In Chap.3, we develop a new optical TDM scheme using soliton interaction. Followed is the optimal solution in terms of the TBP, where the parameters can be modified to simulate a linear or quasi-linear environment. The simulation result shows that the proposed soliton multiplexing scheme can save the TBP about 4.1% in terms of sequences, and therefore provides a higher Q factor compared with the conventional TDM scheme.

There exists, however, a drawback with the above scheme. That is, when it is used in a conventional TDM environment, the composite soliton occupies a large period in time domain, which will reduce the multiplexing capacity in terms of the original inputs. Therefore, a modified scheme is introduced in chap.4 with a modified soliton interaction implementation. Compared with the previous scheme, the modified system can provide a higher TBP saving and is suitable for the conventional TDM use. Accurate modeling of the effects of additive white Gaussian noise (AWGN) on the dynamics of the modified scheme is given later. The simulation result shows that the modified soliton multiplexing scheme has a $3.7dB$ lower bit error rate (BER) than the conventional TDM scheme, while keeping the same total bit rate.

Finally, Chap.5 summarizes the main contributions of the thesis and indicates some interesting directions for future study.

Chapter 2

Background and Related Work

Solitons [3,4] are solutions to a special class of nonlinear partial differential equations representing certain nonlinear systems. They are a kind of stable, pulse-like signals which can transmit in nonlinear media for a long distance without any distortion in ideal conditions. Because of their perfect performance against perturbation, solitons have been widely employed in optical communications [5] as information carriers.

The history of solitons dates back to the dsicovery of John Scott Russell in 1834. What Scott Russell actually observed was a solitary wave solution to what is now known as the Korteweg-de Vries (KdV) equation. The research of solving soliton systems began with the work of C. S. Gardner, *et. al.* [6] on the KdV equation. These techniques were generalized by P. D. Lax and then by M. A. Ablowitz *et. al.* [7] and used to solve what is now a large class of solvable nonlinear evolution equations.

Although there are no new results presented here, this chapter serves as an introduction to solitons and to a kind of important nonlinear system that supports fiber solitons, described by the NSE.

2.1   Nonlinear Schrödinger Equation

The mathematical description of fiber solitons requires solution to the wave equation in a dispersive nonlinear medium. A general approach is to employ the well-known NSE,

$$\frac{\partial A}{\partial z} + \beta_1 \frac{\partial A}{\partial t} + \frac{i}{2}\beta_2 \frac{\partial^2 A}{\partial t^2} - \frac{1}{6}\beta_3 \frac{\partial^3 A}{\partial t^3} = i\gamma|A|^2 A - \frac{\alpha}{2}A \qquad (2.1)$$

where $A(z,t)$ is the amplitude of the pulse envelope, z is the transmission length, t is the time, β_1, β_2 and β_3 represent, respectively, the inverse group velocity, the group velocity dispersion (GVD) and the third-order dispersion, γ is the nonlinear coefficient and α is the fiber attenuation factor. This is the basic propagation equation that governs pulse evolution inside a single mode fiber. Specially, when the pulse-width is not too small ($\geq 5ps$), the third-order dispersion, β_3, can be ignored. Making the transformation to a reference frame moving with the pulse and introducing the new coordinates

$$T = t - \beta_1 z$$

Eq.(2.1) can be written as

$$i\frac{\partial A}{\partial z} = \frac{1}{2}\beta_2\frac{\partial^2 A}{\partial T^2} - \gamma|A|^2 A - \frac{i}{2}\alpha A \tag{2.2}$$

Let us consider the loss-free case, $\alpha = 0$. It is useful to normalize Eq.(2.2) by introducing

$$U = \frac{A}{\sqrt{P_0}}, \qquad \xi = \frac{z}{L_D}, \qquad \tau = \frac{T}{T_0}$$

and obtain

$$i\frac{\partial U}{\partial \xi} = \text{sgn}(\beta_2)\frac{1}{2}\frac{\partial^2 U}{\partial \tau^2} - N^2|U|^2 U \tag{2.3}$$

where P_0 is the pulse peak power, T_0 is a measure of the pulse-width, and the parameter N is defined by

$$N^2 = \frac{L_D}{L_{NL}} = \frac{\gamma P_0 T_0^2}{|\beta_2|} \tag{2.4}$$

with the dispersion length L_D and the nonlinear length L_{NL} given by

$$L_D = \frac{T_0^2}{|\beta_2|}, \qquad L_{NL} = \frac{1}{\gamma P_0}$$

In the case of anomalous dispersion, $\text{sgn}(\beta_2) = -1$, Eq.(2.3) takes the following standard form:

$$i\frac{\partial U}{\partial \xi} = -\frac{1}{2}\frac{\partial^2 U}{\partial \tau^2} - N^2|U|^2 U \tag{2.5}$$

2.2   Fiber Solitons

Mathematical analysis on Eq.(2.5) shows that if an input pulse with an initial waveform

$$U(0,\tau) = N\text{sech}(\tau)\exp(i\theta) \tag{2.6}$$

is launched, its shape remains unchanged during propagation when $N = 1$, which is called the *fundamental soliton*. The parameter N represents the order of the soliton. In the context of optical fibers, the solution (2.6) indicates that if a *hyperbolic-secant* pulse is launched, whose width T_0 and the peak power P_0 are chosen such that $N = 1$, the pulse will propagate undistorted in shape for an arbitrarily long distance in ideal conditions.

It is this feature of the fundamental soliton that makes it attractive for information transmission in optical communication systems. Fig 2.1 shows the evolution form of the fundamental soliton in optical fibers.
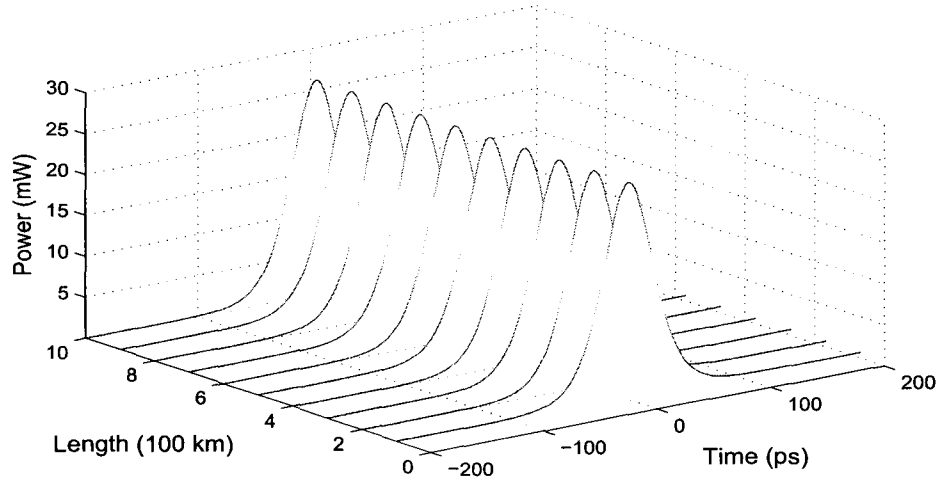
Figure 2.1: Evolution of the fundamental soliton in fibers

2.3   Characteristics of Fiber Solitons

2.3.1   Power Requirement

The peak power P_0 required to support a fundamental soliton is obtained by setting $N = 1$ in Eq.(2.4) and given by

$$P_0 = \frac{|\beta_2|}{\gamma T_0^2} \simeq \frac{3.11|\beta_2|}{\gamma T_{FWHM}^2}$$

where the full width at half maximum (FWHM)

$$T_{FWHM} = 2T_0 \ln(1 + \sqrt{2}) \simeq 1.763 T_0$$

is commonly used in practice, and also throughout this thesis, as a measure of the pulse-width.

7

2.3.2   Higher-Order Solitons

When $N\mathrm{sech}(\tau)\exp(i\theta)$ is launched into the fiber, its shape follows a periodic pattern for integer values $N > 1$ such that the input shape is recovered at $\xi = m\pi/2$, where m is an integer. The optical pulses corresponding to $N > 1$ are called *higher-order solitons*. By noting that $\xi = z/L_D$, the soliton period z_p, defined as the distance over which higher-order solitons recover their original shapes, is given by

$$z_p = \frac{\pi}{2}L_D = \frac{\pi}{2}\frac{T_0^2}{|\beta_2|} \tag{2.7}$$

Fig 2.2 shows the evolution form of the higher-order soliton in optical fibers.
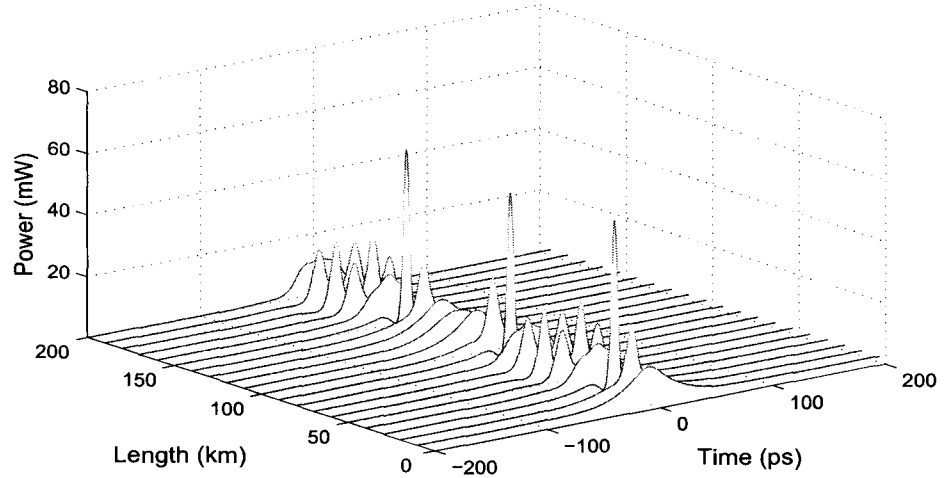
Figure 2.2: Evolution of the higher-order soliton in fibers

2.3.3   Stability

An important property of fiber solitons is that they are remarkably stable against perturbations. Though the fundamental soliton requires a specific shape and a certain peak power corresponding to $N = 1$ in Eq.(2.6), it can be created even when the pulse shape and the peak power deviate from accurate conditions. Fig 2.3 shows the numerically

simulated evolution of a Gaussian pulse for which $U(0, \tau) = \exp(-\tau^2/2)$. As seen there, the pulse adjusts its shape and width in an attempt to become a fundamental soliton and will attain a *hyperbolic-secant* profile for $\xi \gg 1$.
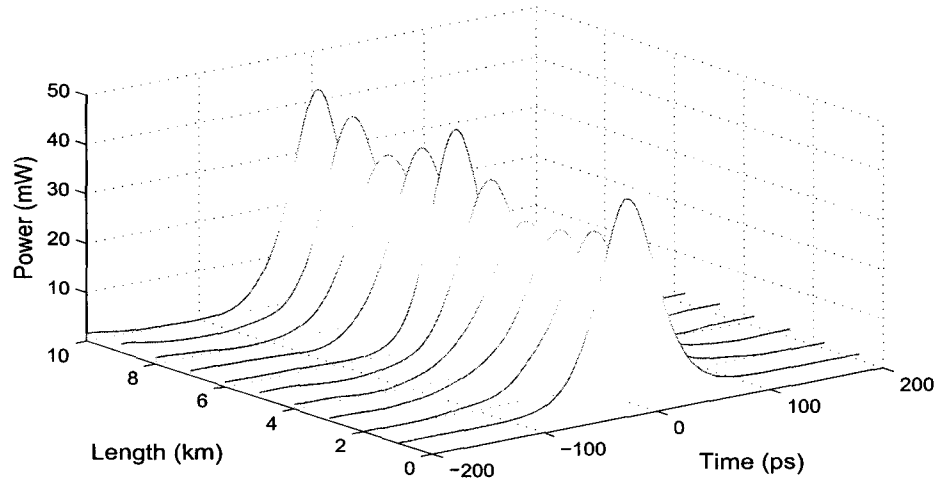
Figure 2.3: Evolution of the Gaussian pulse in fibers

A similar behavior occurs when N deviates from 1. It turns out that the Nth-order soliton can be formed when the input value of N is in the range of $\left(N - \frac{1}{2}, N + \frac{1}{2}\right)$. In particular, the fundamental soliton can be excited for values of N in the range of $(0.5, 1.5)$. Fig 2.4 shows the pulse evolution over the range $\xi = 0 \sim 10$ by solving the NSE with the initial condition $U(0, \tau) = 1.2\mathrm{sech}(\tau)$. The pulse width and the peak power oscillate initially but eventually become constant after the input pulse has adjusted itself to satisfy the condition of $N = 1$.

2.4   Soliton Interaction

Mathematically, the soliton in Eq.(2.6) is valid only when $-\infty < \tau < \infty$. It remains approximately valid for a sequence of solitons only when they are well isolated. This
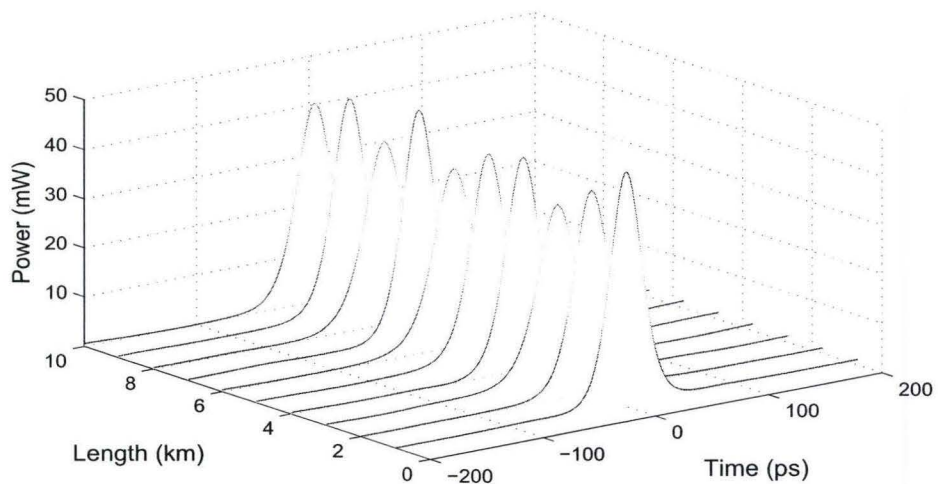
Figure 2.4: Evolution of the *sech* pulse in fibers with N deviated from 1

requirement can be used to relate the soliton width T_{FWHM}, or T_0, to the bit rate B as

$$B = \frac{1}{T_B} = \frac{1}{2\tau_0 T_0} \simeq \frac{0.88}{\tau_0 T_{FWHM}} \tag{2.8}$$

where T_B is the duration of the bit slot and $2\tau_0 = T_B/T_0$ is the separation between neighboring solitons in the normalized unit.

The presence of pulses in the neighboring bits perturbs a temporal soliton simply because the combined optical field is not an exact solution to the NSE. Neighboring solitons either come closer or move apart because of a nonlinear interaction between them, which is so called *soliton interaction*. In a special case, when two identical fundamental solitons interact in a nonlinear medium, they may interact to form a *composite soliton* which, if continued to be processed by the nonlinear medium, will be resolved into its component solitons again without distortion. This is the very point behind our soliton multiplexing scheme that will be discussed in Chap.3.

One can understand the implication numerically, with the input amplitude consisting of a soliton pair such as

$$U(0, \tau) = \text{sech}(\tau - \tau_0) + r\text{sech}[r(\tau + \tau_0)] \exp(i\theta) \tag{2.9}$$

10

where r is the relative amplitude, θ is the relative phase, and $2\tau_0$ is the initial separation. Clearly, soliton interaction depends strongly on r, θ and τ_0.

2.4.1 Interaction between Identical Solitons

Consider first the case of interaction between identical fiber solitons. In the specific case of $r = 1$ and $\theta = 0$, Eq.(2.9) can be rewritten as

$$U(0, \tau) = \text{sech}(\tau - \tau_0) + \text{sech}(\tau + \tau_0) \tag{2.10}$$

Since it satisfies the *in-phase* condition, the two solitons will attract each other such that they collide periodically along the fiber length. From the inverse scattering transform (IST) method [3, 4], the soliton separation $2\tau_s$ at any length ξ is given by

$$2\exp[2(\tau_s - \tau_0)] = 1 + \cos[4\xi \exp(-\tau_0)]$$

This relation shows that the spacing $2\tau_s(z)$ between two neighboring solitons oscillates periodically with the period

$$\xi_p = \frac{\pi \sinh(2\tau_0) \cosh(\tau_0)}{2\tau_0 + \sinh(2\tau_0)} \tag{2.11}$$

Fig 2.5 shows the interaction between two identical fundamental solitons in optical fibers.

2.4.2 Soliton Interaction with Unequal Amplitudes

From the IST analysis, we know that a single soliton propagates along the fiber with a phase change proportional to its amplitude square and the distance. Therefore, the phase of a larger amplitude soliton will change faster. When two solitons are launched with unequal amplitudes but equal initial phases, the phase difference between them will change periodically along the distance, from attraction to repulsion. The two pulses may then maintain their relative position while exhibiting small periodic oscillations.

Figure 2.5: Evolution of soliton interaction in fibers

When launching two unequal amplitude pulses, consider the initial pulse waveform such as

$$U(0, \tau) = \text{sech}(\tau - \tau_0) + r\text{sech}\left[r(\tau + \tau_0)\right].\tag{2.12}$$

Fig 2.6 shows the evolution of two fundamental solitons having unequal amplitudes with $r = 1/\sqrt{2}$.

Since the two pulses exhibit small periodic oscillations, we need to know the separation of the pulses along the fiber length. The maximum separation equals the initial separation, $2\tau_0$, and the separation along the fiber length can be obtained from the IST [24] as

$$\begin{aligned}
\Delta\tau &= k\ln\left(\exp(\tau_0/k) + \frac{2}{a^2}\left[\cos(2a\xi) - 1\right]\right) \tag{2.13}\\[2mm]
a &= \left[4\exp(-\tau_0/k) + \left(\frac{r-1}{r+1}\right)^2\right]^{1/2}\\[2mm]
k &= \frac{r+1}{4r}
\end{aligned}$$

Fig 2.7 shows the separation between two fundamental solitons with unequal amplitudes, initially separated by $2\tau_0 = 3.5\, T_{FWHM}/T_0$ and with $r = [\frac{1}{\sqrt{3}}, \frac{1}{\sqrt{2}}, \frac{1}{1.1}, 1, 1.1, \sqrt{2}, \sqrt{3}]$.

12
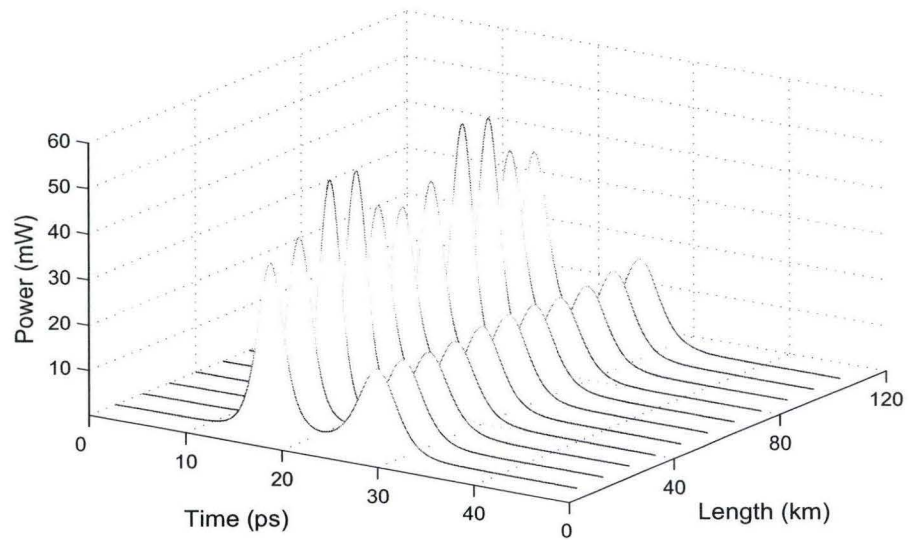
Figure 2.6: Evolution of the soliton pair with unequal amplitudes
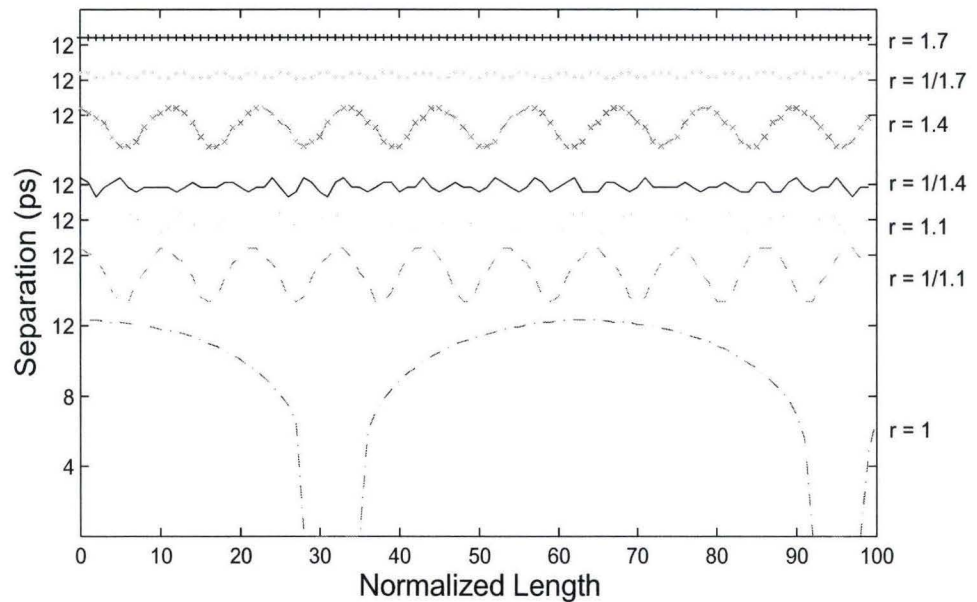
Figure 2.7: Separation between two solitons with unequal amplitudes

13

2.4.3 Soliton Interaction with Unequal Phases

When launching two unequal phases pulses, consider the initial pulse waveform such as

$$U(0, \tau) = \text{sech}(\tau - \tau_0) + \text{sech}(\tau + \tau_0) \exp(i\theta). \tag{2.14}$$

For small values of θ, the separation of the solitons as a result of the finite velocity difference will counteract the effect of the oscillation which tries to bring the two together. The propagation of two solitons is shown in Fig 2.8, where the initial phase difference is $\theta = \pi/3$ and the separation is $2\tau_0 = 3.5 \, T_{FWHM}/T_0$. We can see that the solitons separate from each other after an initial attraction stage.
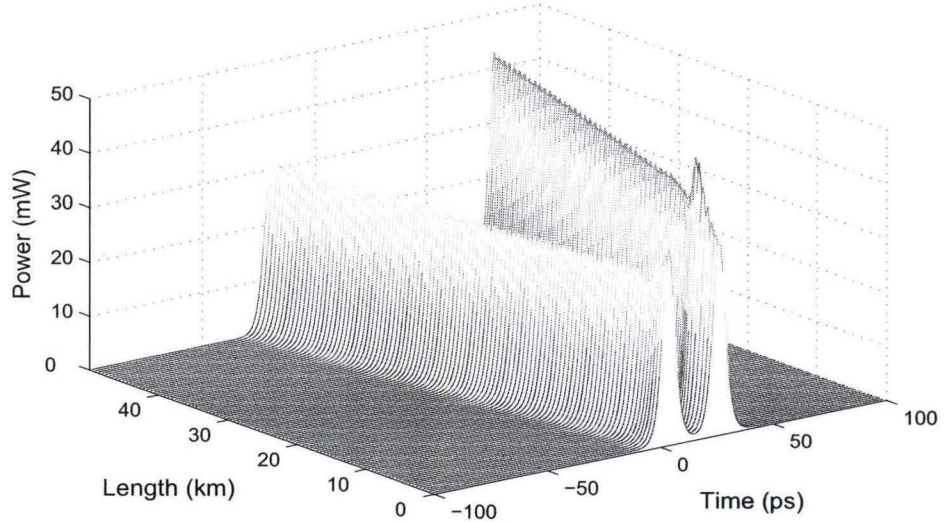
Figure 2.8: Evolution of the soliton pair with unequal phases

From the IST, an approximate expression for pulse separation as a function of the distance along the fiber can be obtained [24],

$$\begin{aligned}
\cdot \Delta\tau &= \tau_0 + \frac{1}{2} \ln \left[\frac{\cosh(2v\xi) + \cos(2a\xi)}{2} \right] \\
a &= 2 \exp(-\tau_0) \cos(\theta/2) \\
v &= -2 \exp(-\tau_0) \sin(\theta/2).
\end{aligned} \tag{2.15}$$

14

It can be seen from Fig 2.9 that introducing a phase difference results in the eventual separation of the pulses. Increasing the phase difference causes the solitons to repel each other even more strongly. For $\theta > \pi/2$, no oscillation is observed.
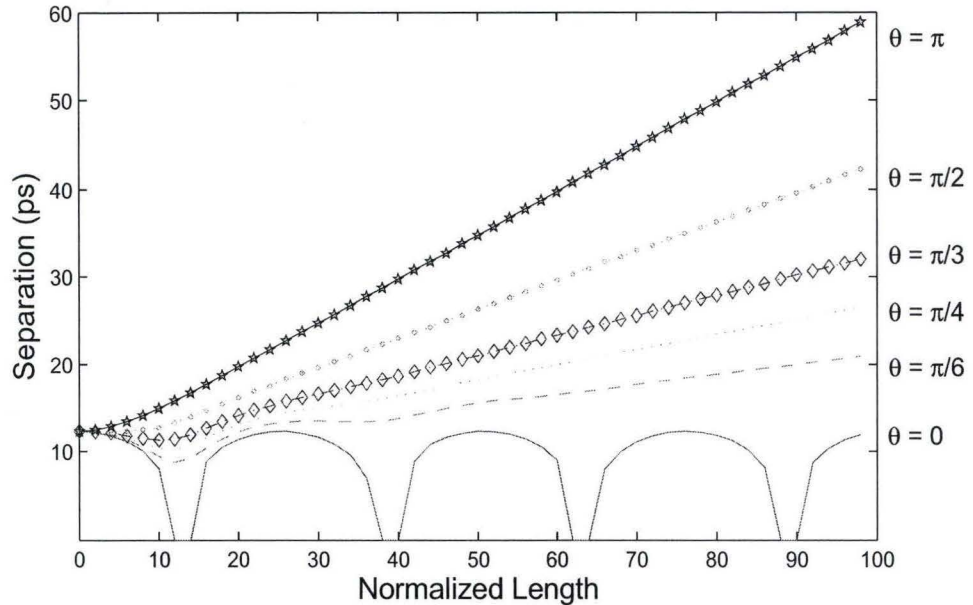
Figure 2.9: Separation between two solitons with unequal phases

From the standpoint of system design, such behavior is not acceptable. It would lead to jitter in the arrival time of solitons because the relative phase of neighboring solitons is not likely to remain well controlled. One way to avoid interaction is to increase $2\tau_0$ because the strength of interaction depends heavily on the initial separation. For sufficiently large $2\tau_0$, deviations in the soliton position are expected to be small enough that the solitons remain at their initial positions within the bit slots over the entire transmission distance.

Chapter 3

Optical Time Division Multiplexing Scheme Using Soliton Interaction

3.1   Theory of Multiplexing Using Soliton Interaction

As shown in Chap.2, one important property possessed by solitons is that when two temporally separated fundamental solitons interact, they may combine to generate a single pulse, which we call *composite soliton*, at the collision distance $z_c = 0.5z_p$ and the component solitons will be restored at z_p without any distortion in idea conditions [3,4]. We make use of this property to design a soliton multiplexing scheme, as shown in Fig 3.1.
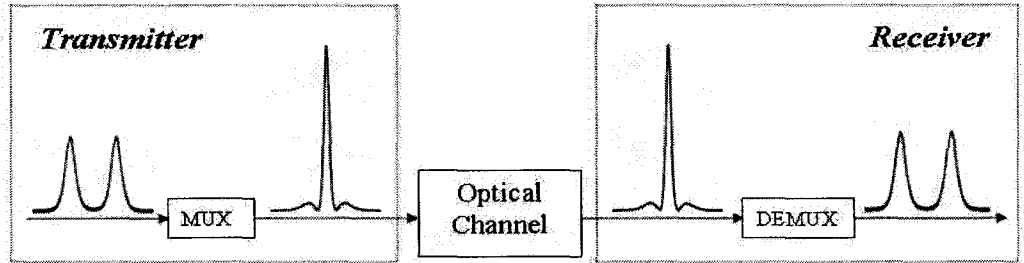
Figure 3.1: Concept of the multiplexing scheme using soliton interaction

At the transmitter part, two fundamental solitons are launched into a soliton MUX to generate a composite soliton, which will be transmitted over an optical channel. At the receiver part, the composite soliton passes through a bandpass filter and then a Soliton DEMUX similar to that at the transmitter part, which demultiplexes the composite soliton to restore the component fundamental solitons. In the case of a quasi-linear channel, an attenuator, to modify the signal's power suitable for nonlinear transmission, and a corresponding amplifier are necessary at the transmitter and the receiver parts, respectively.

The TBP is generally used as a measure to assess the temporal and spectral confinement of a signal. The TBP for an arbitrary signal $f(t)$ is defined as

$$TBP = \sigma_t \cdot \sigma_\omega \qquad (3.1)$$

17

where

$$\sigma_t = \sqrt{\frac{1}{E}\int_{-\infty}^{\infty} t^2|f(t)|^2 dt}$$

$$\sigma_\omega = \sqrt{\frac{1}{2\pi E}\int_{-\infty}^{\infty} \omega^2|F(\omega)|^2 d\omega}$$

$$E = \int_{-\infty}^{\infty} |f(t)|^2 dt = \frac{1}{2\pi}\int_{-\infty}^{+\infty} |F(\omega)|^2 d\omega$$

Here we choose two identical fundamental solitons with $T_{FWHM} = 5\ ps$. The initial separation between them is chosen to be $2.5T_{FWHM}$. The parameters of the soliton MUX fiber are chosen as follows: dispersion $D = 1.7\ ps/nm/km$, nonlinear coefficient $\gamma = 7.5\ W^{-1} \cdot Km^{-1}$. Fig 3.2 shows the TBP as a function of the soliton MUX fiber's length. As can be seen, the minimum TBP is found to be 0.8708 at 17.6 km, which occurs before the collision distance, $z_c = 24.14\ km$.
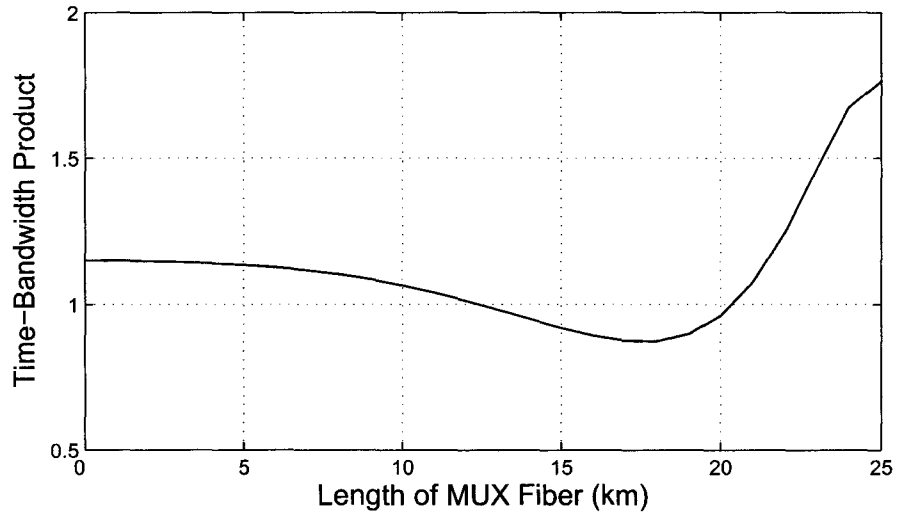
Figure 3.2: TBP for different soliton MUX lengths

Fig 3.3 shows, respectively, the initial waveform and the pulse envelop at the transmission point where the TBP is minimum.
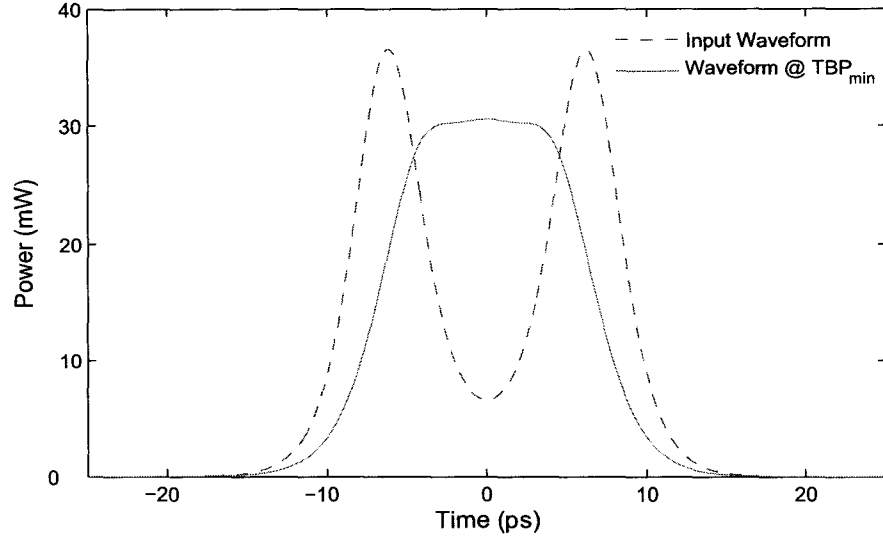
Figure 3.3: Initial waveform *vs.* Min-TBP pulse envelop

Table 3.1 shows the simulation results, where B_{FWHM} and $B_{99\%}$ correspond to the full widths at 50% and 99% of the peak power, respectively.

Table 3.1: Comparison of fundamental and composite solitons

Solitons		Fundamental	Composite
T_{FWHM}	(ps)	5.00	14.30
B_{FWHM}	(GHz)	62.97	41.25
$B_{99\%}$	(GHz)	189.06	186.72
σ_t	(ps)	2.57	4.87
σ_f	(GHz)	32.40	28.60

Using Eq.(3.1), the TBP_F of the fundamental soliton and the TBP_C of the composite soliton are calculated such as

$$TBP_F = 0.5236 \qquad\qquad (3.2a)$$

$$TBP_C = 0.8708 \qquad\qquad (3.2b)$$

Comparing Eq.(3.2a) with Eq.(3.2b), we find that the TBP_C is about 83.16% of

19

$2 \times TBP_F$, which indicates that the composite soliton has a higher time-frequency localization ability. Though, in principle, two pulses can be linearly superposed to obtain more minimum TBP, it would not be possible to separate them at the receiver part.

3.2   Optical TDM Scheme Using Soliton Interaction

Based on the above property of solitons, we propose an optical soliton multiplexing scheme, whose schematic is shown in Fig 3.4.
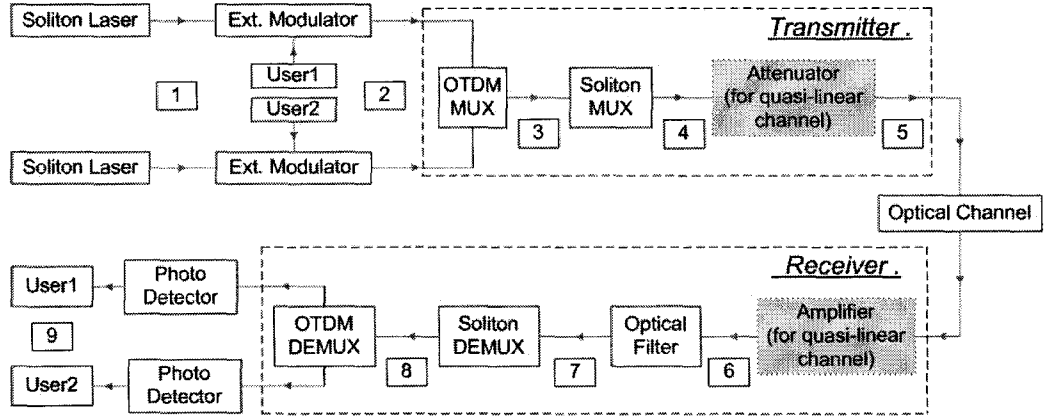
Figure 3.4: Schematics of the optical TDM scheme using soliton interaction

Here *Soliton Laser* generates an all-'1' sequence with each bit represented by a fundamental soliton. *User1* and *User2* account for different data sources in electrical domain, which modulate the all-'1' sequence inputs to the external modulators through *on-off keying* (OOK) to get the desired '1'/'0' sequences in optical domain. The outputs of the two external modulators are linearly multiplexed (at OTDM MUX) in time domain first and then passed through a soliton MUX. Two adjacent solitons at the input of the soliton MUX are combined to form a composite soliton. The output of the soliton MUX will be attenuated, and correspondingly amplified later at the receiver part, if the signal is transmitted over a quasi-linear channel. At the receiver part, the signal is passed through an ideal bandpass filter to suppress noises. After the filter, the signal passes through the

soliton DEMUX to restore the component solitons, which will be demultiplexed using the following conventional OTDM DEMUX to separate *User1* and *User2*.

3.2.1 Linear Channels

For convenience, we first concentrate on the case of linear transmission channels. An example for linear channels is the free space propagation. The following parameters are used in this simulation: wavelength $\lambda = 1550$ nm, bit rate of *User1* or *User2*, $B = 20$ Gb/s, initial hyperbolic-secant pulses with $T_{FWHM} = 5$ ps. Dispersion of the soliton MUX and DEMUX fibers $D = 1.7$ $ps/nm/km$, nonlinear coefficient $\gamma = 7.5$ $W^{-1} \cdot Km^{-1}$. Before the OTDM MUX, the data of *User2* is shifted by 2.5 T_{FWHM} so that only the nearest solitons interact. The bit sequence of every user consists of 1024 bits with equal probability for '1' and '0'. Bit '1' is transmitted by sending a fundamental soliton with peak power P_0, and bit '0' is transmitted by sending nothing. The additive white Gaussian noise (AWGN) in the transmission channel has a power spectral density (PSD) of $\rho = -150$ dBm/Hz. The bandpass filter at the receiver part has a single-side pass bandwidth of $B_{pass} = 140$ GHz. The bit pattern at the various stages of this scheme is shown in Fig 3.5. Fig 3.6 shows the eye-diagram of *User1* at the OTDM DEMUX (point 9 in Fig 3.4).
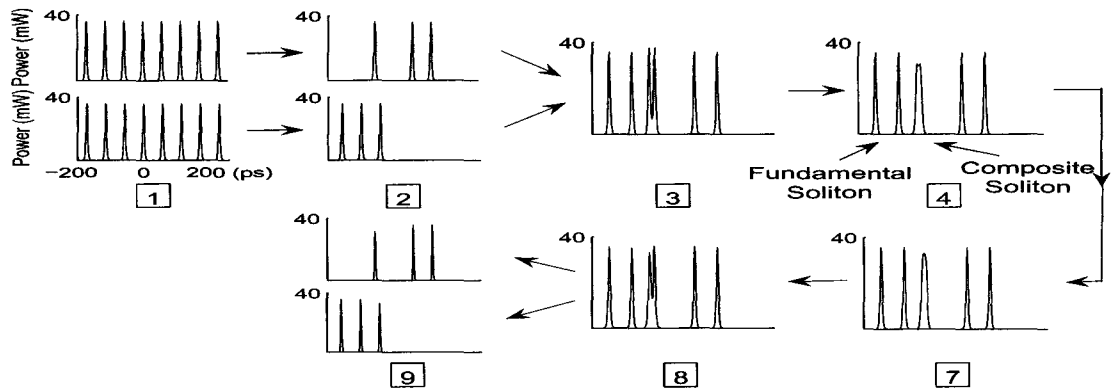
Figure 3.5: Signal flow chart through linear channels
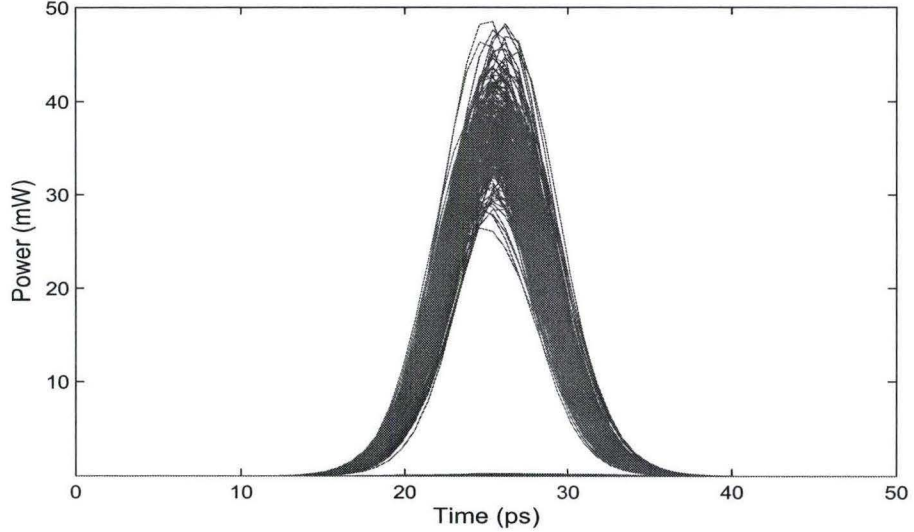
Figure 3.6: The eye-diagram of *User1* after linear channels

According to Eq.(3.2a) and Eq.(3.2b), the TBP of the composite sequence after the soliton MUX, corresponding to point 4 in Fig 3.4, is

$$TBP_{Sequence} = \frac{1}{4}TBP_C + \frac{1}{2}TBP_F + \frac{1}{4} \times 0 = 0.4795 \qquad (3.3)$$

since the composite and the fundamental solitons occupy, respectively, $\frac{1}{4}$ and $\frac{1}{2}$ of the total bits. Compared to a conventional 40 *Gb/s* system using Gaussian pulses with the same input average power, which has the minimum TBP = 0.5, we obtain a saving of 4.10% in terms of TBP with this optical OTDM scheme using soliton interaction.

3.2.2 Quasi-Linear Channels

For the proper operation of the proposed scheme, the transmission channel should be linear. In the thesis, however, we show that the proposed scheme also works reasonably well for quasi-linear transmission in optical fibers if the launch power is not too large.

The quasi-linear transmission is modeled using the following parameters. Dispersion of the pre-compensation and the post-compensation fibers is $D_{comp} = -100\ ps/nm/km$.

Dispersion management is achieved by using $L = 40\ km$ of standard single-mode fiber with dispersion $D_+ = 17\ ps/nm/km$ followed by a negative dispersion fiber with dispersion $D_- = -14.5\ ps/nm/km$, of the same length. The total length of the pre- and post-compensation fibers is chosen such that the accumulated dispersion at the receiver is zero. Fiber attenuation $\alpha = 0.2\ dB/km$, amplifier spacing $L_{amp} = 80\ km$, amplifier noise figure $NF = 5.5\ dB$, inline amplifier gain $G = 16\ dB$. An AWGN with a PSD $\rho_{ASE} = hc/\lambda \times (G \times NF - 1)$ is introduced at each amplifier site. Fig 3.7 shows the eye-diagram of *User1* at the output of the OTDM DEMUX (point 9 in Fig 3.4) after a $400\ km$ quasi-linear channel. The launch power to the quasi-linear channel is $2\ mW$.
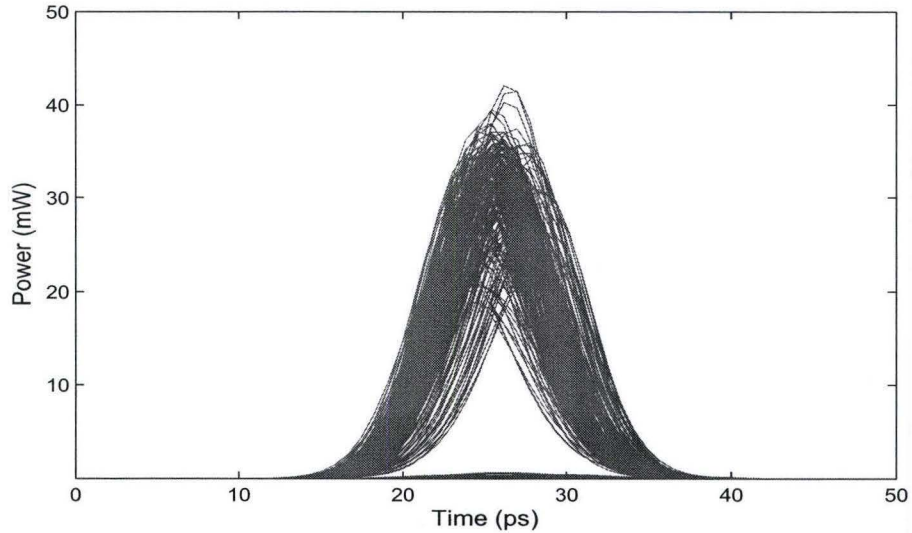
Figure 3.7: The eye-diagram of *User1* after quasi-linear channels

3.2.3 Soliton DEMUX Length

For a linear channel, the length of the HNLF at the soliton DEMUX is $30.68\ km$ so that, according to Eq.(2.11), the total length of the HNLF at the soliton MUX and the soliton DEMUX is equal to the soliton period $z_p = 48.28\ km$. However, for the quasi-linear channel, because of the nonlinear phase shift introduced by the transmission fibers, the

23

separation between the component solitons at the receiver part is no longer kept the same with that at the transmitter part. Fig 3.8 shows the maximum separation, corresponding to the point where component solitons are taken as receiver output, as a function of the peak power launched into the quasi-linear channel, where we can see that as the peak power increases, the separation decreases. This is just because that the nonlinear phase changes proportional to its amplitude square. The larger the peak power, the heavier the nonlinear interaction. Therefore, the component solitons are bounded together more than the case of linear channels. Specially, when the peak power is larger than 3 mw, there is no separation observed at the receiver part.
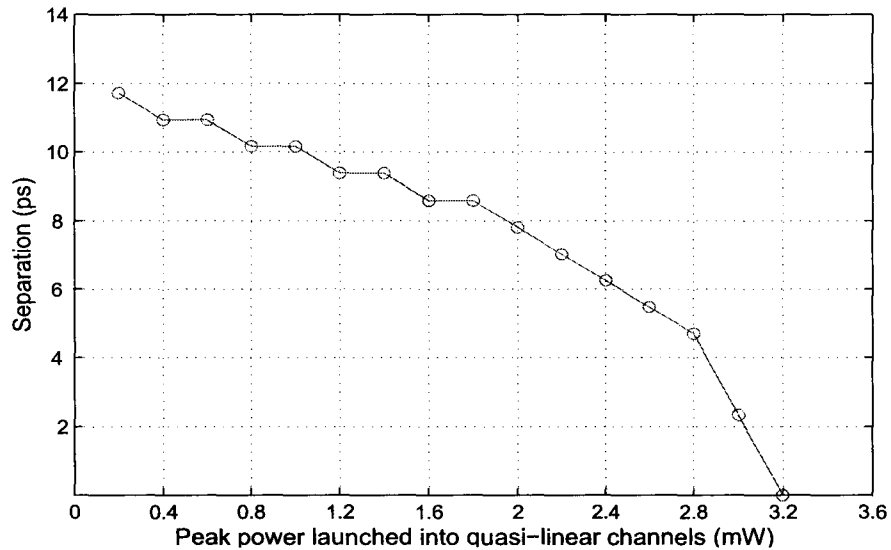
Figure 3.8: Separation between component solitons at the receiver part when different P_{peak} is launched into quasi-linear channels

Since the maximum separation varies with the peak power, the length of the HNLF at the soliton DEMUX needs to be adjusted. Fig 3.9 shows the length of the soliton DEMUX fiber as a function of the peak power. As can be seen, the length reduces as the peak power increases, since the separation reduces because of the additional nonlinear phase shift introduced by the quasi-linear channel. Fig 3.10 gives out a special case of the

24

evolution of the composite soliton at the soliton DEMUX when the peak power is chosen to be $2\ mW$.
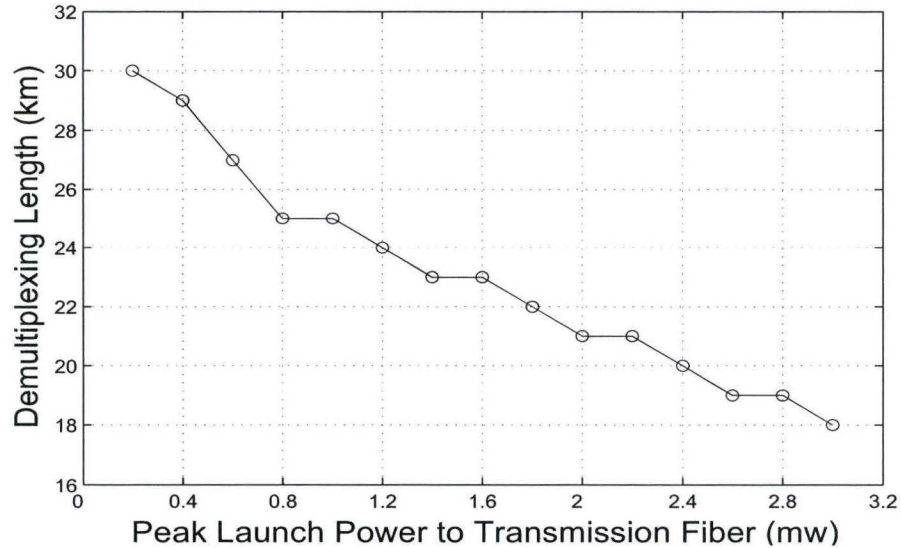
Figure 3.9: Soliton DEMUX lengths for different P_{peak} launched into quasi-linear channels

Fig 3.11 shows the Q factor at the receiver under different peak powers, compared with the conventional TDM scheme using Gaussian pulses having both the same total bit rate, and peak, as well as average, powers.

3.2.4   Different '1'/'0' Distribution

We note that the saving of 16.84% in TBP is obtained for a single soliton pair. The savings in TBP can be increased by increasing the number of users or increasing the '1'/'0' distribution larger than 50%/50% corresponding to each user.

25
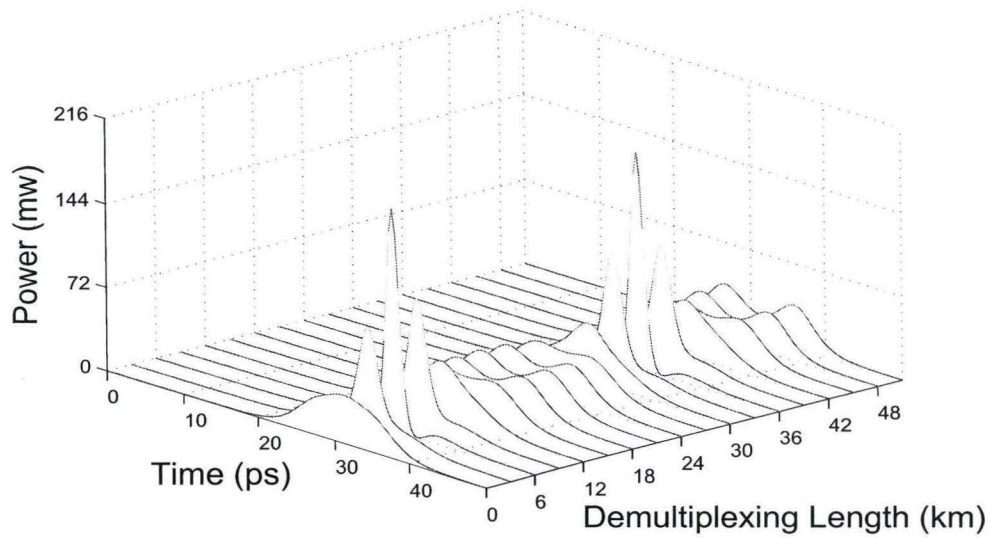
Figure 3.10: Evolution of the composite soliton at the soliton DEMUX with $P_{peak} = 2mW$
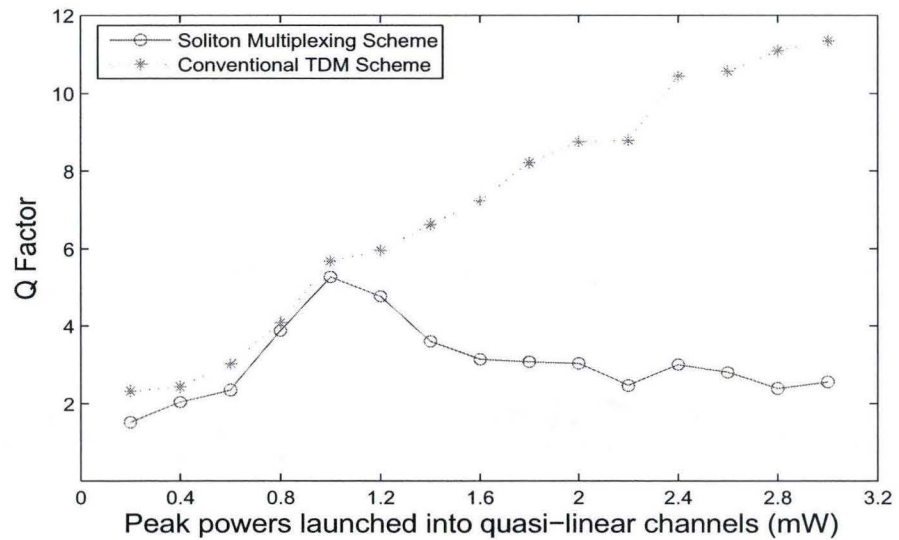
Figure 3.11: Q factor under different P_{peak} launched into quasi-linear channels

Chapter 4

Modified Optical Time Division Multiplexing Scheme Using Soliton Interaction

4.1   Drawback of the Optical TDM Scheme

Though we can obtain TBP saving from the previous scheme in Chap.3, it is noted that such a benefit can only be achieved when the total user number is not more than 5. The reason can be shown in Fig 4.1.
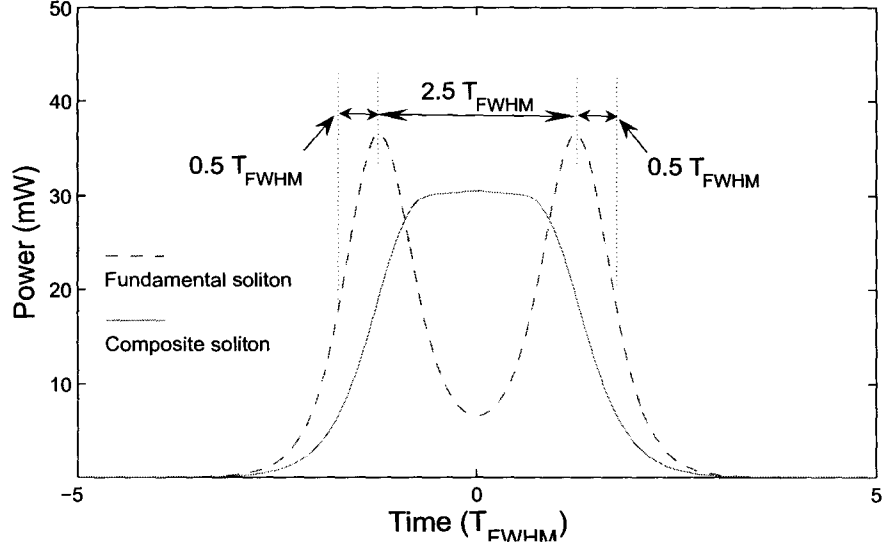
Figure 4.1: Time window occupation within one period $T_B = 10 \, T_{FWHM}$

If the center point of the *User1* pulses is taken as 0, then the center point of the *User2* pulses is at 2.5 T_{FWHM} away. Since $T_B = 10 \, T_{FWHM}$ here, and there are no signals other than *User1*, *User2* or the composite pulses can occupy the temporal window of $(0.5 + 2.5 + 0.5) \, T_{FWHM} = 3.5 \, T_{FWHM}$, therefore only another 3 more users at most can be multiplexed within the whole time period of T_B, which means less channels than the conventional TDM can be multiplexed in this scheme. Therefore, although the TBP of a composite soliton is smaller than that of two linear pulses used in conventional TDM systems, the number of channels cannot be increased beyond that used in the conventional TDM scheme. Instead, we propose a modified scheme in which the reduction in TBP can translate into either savings in bandwidth or increase in the number of users for the same bandwidth.

Since the information contained in *User1* and *User2* is known *a priori*, we can take an electrical pre-process before the OTDM MUX to facilitate later TDM steps. That is, if *User1* and *User2* both have bits '1' in the same T_B, we can select the composite soliton as the output from the soliton MUX at the point where its TBP is minimum. Otherwise, if both are not '0', the user bits '1' are shifted in time so that their center points are of the same with that of the composite soliton. Therefore, the composite sequence may provide a higher multiplexing capacity than the scheme proposed in Chap.3.

However, there comes up another problem with this modification. That is, within a certain T_B, there are four kinds of composite pulses, i.e., '00', '11', '01', and '10'. Here, if we choose identical fundamental solitons for bits '1' in *User1* and *User2*, it will be impossible to tell '01' from '10' at the receiver part, that is, *User1* and *User2* cannot be detected correctly.

4.2 Soliton Interaction with Unequal Amplitudes and Unequal Phases

From Chap.2, we know that the two solitons with either unequal amplitudes or unequal phases are widely used in engineering to prevent from interaction. Therefore, it is straightforward for us to use the reverse concept to generate the composite pulse from two fundamental solitons with both unequal amplitudes and unequal phases. Fig 4.2 shows the separation between two fundamental solitons with both unequal amplitudes ($r = 1/\sqrt{2}$) and unequal phases. We can see here that the larger the initial phase difference, the longer the transmission length needed to completely multiplex them.

To facilitate the analysis, we rewrite Eq.(2.9) as follows,

$$U(z,\tau) = \text{sech}(\tau - \tau_0) + r\,\text{sech}\left[r(\tau + \tau_0)\right]\exp(i\theta). \tag{4.1}$$

In a specific case, we let

$$2\tau_0 = 3.5\frac{T_{FWHM}}{T_0} \qquad r = 1/\sqrt{2}, \qquad \theta = \pi/3$$
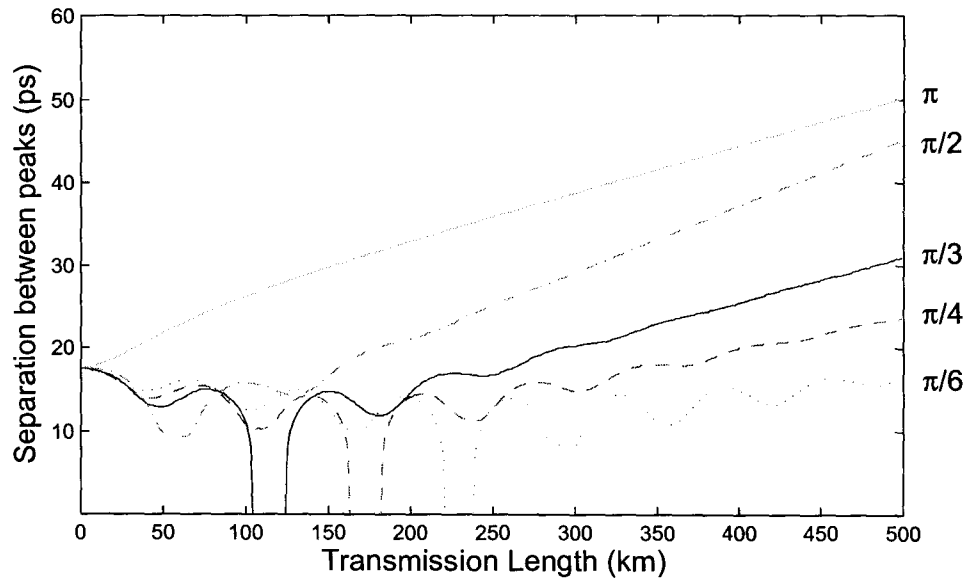
Figure 4.2: Separation between two solitons with unequal amplitudes and unequal phases
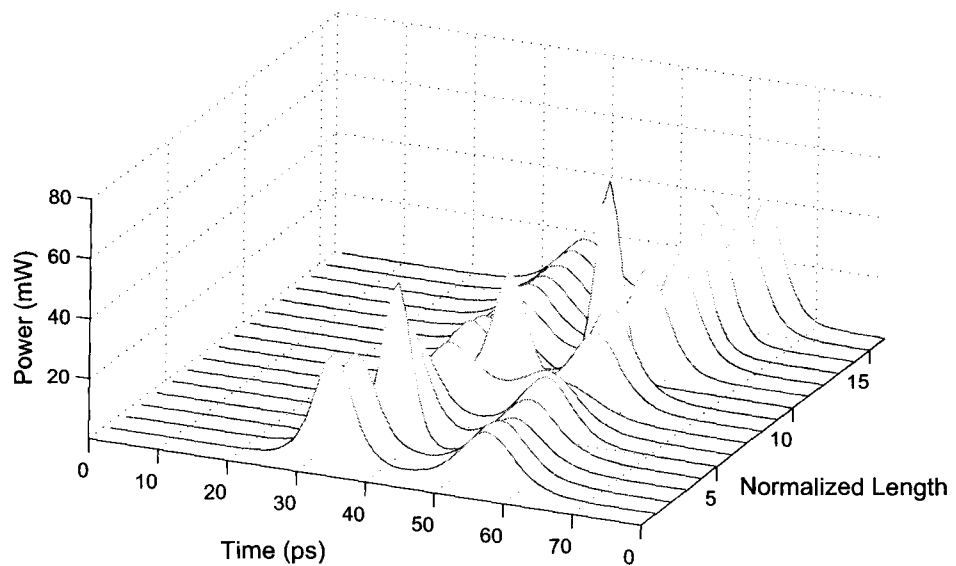
Figure 4.3: Evolution of soliton pair with both unequal amplitudes and unequal phases

Fig 4.3 shows the waveform evolution through the fiber length. From Fig 4.3, we can see that these two fundamental solitons may combine with each other, just like the case between the identical solitons, to form a composite pulse. Fig 4.4 shows the evolution of the TBP of the composite pulse over the fibers, from which we can see that the TBP of the composite soliton reaches the minimum point, $TBP_{min} = 0.7271$, at the length of $L = 124.26\ km$. Fig 4.5 gives out the pulse envelop corresponding to the min-TBP point.
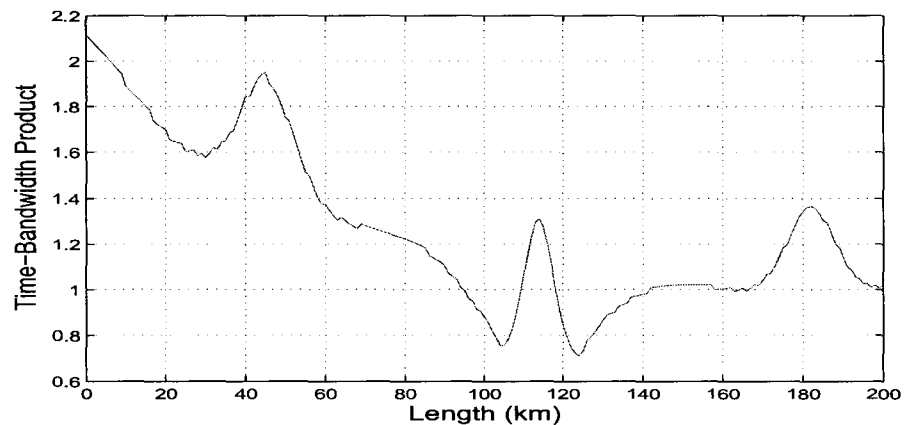
Figure 4.4: TBP evolution over fibers
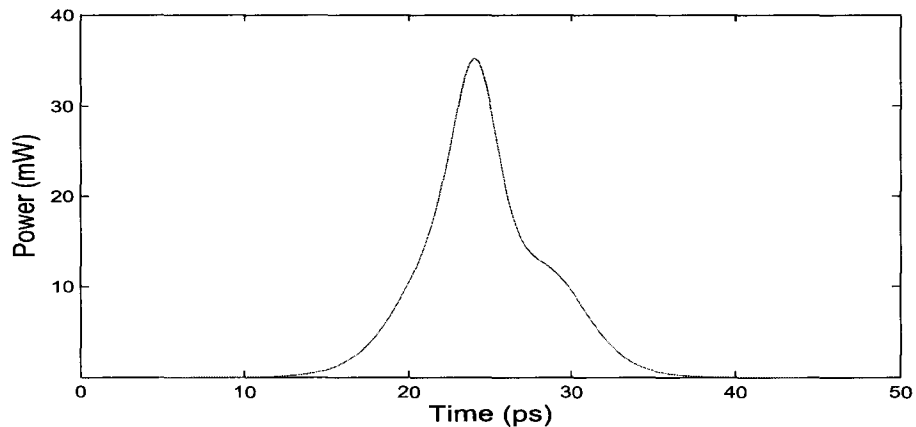
Figure 4.5: Envelops of the composite soliton with the minimum TBP

The simulation result for the min-TBP composite soliton, compared with the input fundamental solitons, is given as follows,

Table 4.1: Comparison of the fundamental solitons and the composite soliton

Solitons		Fundamental 1	Fundamental 2	Composite
T_{FWHM}	(ps)	5.00	7.07	7.07
$B_{99\%}$	(GHz)	189.06	131.12	156.17
σ_t	(ps)	2.57	3.64	4.20
σ_f	(GHz)	32.40	22.91	29.45
TBP		0.5236	0.5236	0.7271

From the last line in Tab.4.1, we can see that the TBPs of the two input fundamental solitons are both 0.5236, the sum of which is larger than that of the single new composite soliton. That is, we can obtain a saving of 30.57% in terms of TBP.

4.3　Modified Optical TDM Scheme

Based on the above property of soliton interaction with unequal amplitudes and unequal phases, we propose a modified multiplexing scheme, as shown in Fig 4.6.
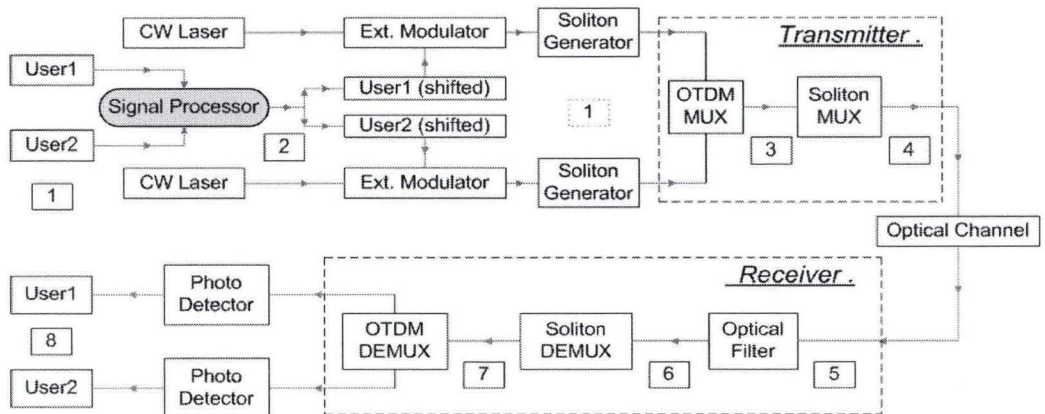
Figure 4.6: Schematics of the modified optical soliton multiplexing system

Different from Fig 3.4, *CW Laser* is used here instead of *Soliton Laser*, since different users employ different fundamental solitons. A pre-signal processor, for example a Field Programmable Gate Array (FPGA), is inserted before the *external modulator*.

1. If '*User1 User2*' is '00' or '11', there is no processing needed;

2. If '*User1 User2*' is '10' or '01', the bit '1' will be shifted a certain time to make sure its center point the same with that of the composite soliton.

Then, as shown in Fig 4.7, the output of the pre-process device has only one kind of center point. All the other parts in this modified scheme are maintained the same with those in Fig 3.4.

(a) before position−shift   (b) after position−shift
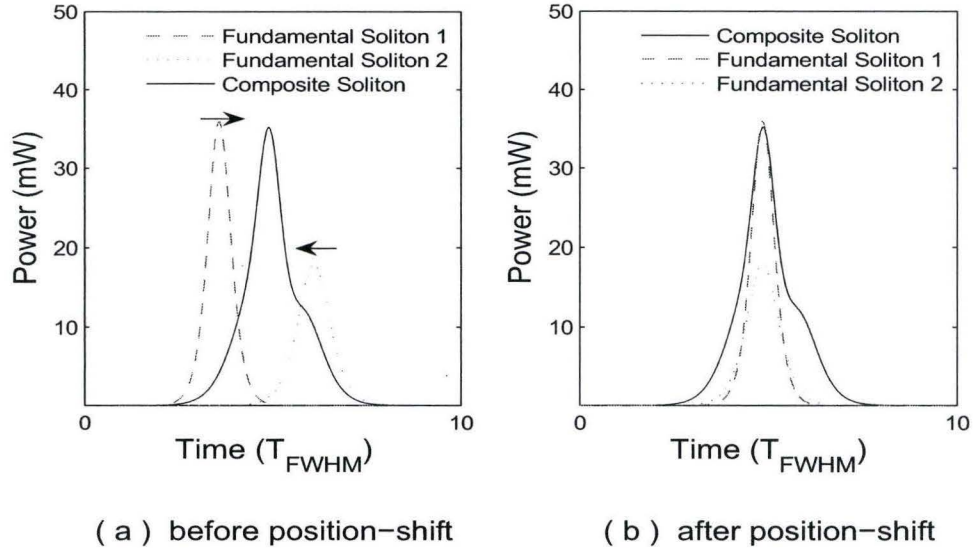
Figure 4.7: Schematics of pulse position shift

The following parameters are used in the modified simulation: wavelength $\lambda = 1550 \, nm$, bit rate of *User1* or *User2*, $B = 20 \, Gb/s$, initial hyperbolic-secant pulses with $T_{FWHM_1} = 5 \, ps$ for *User1*, and $T_{FWHM_2} = 7.07 \, ps$ for *User2*. Dispersion of the soliton MUX and DE-MUX fibers $D = 1.7 \, ps/nm/km$, nonlinear coefficient $\gamma = 7.5 \, W^{-1} \cdot Km^{-1}$. The transmission channel is modeled as a linear environment, with the total length of $400 \, km$. Attenuation $\alpha = 0.2 \, dB/km$, amplifier spacing $L_{amp} = 80 \, km$, amplifier noise figure $NF = 5.5 \, dB$,

33

inline amplifier gain $G = 16\ dB$. An AWGN with a PSD $\rho_{ASE} = hc/\lambda \times (G \times NF - 1)$ is introduced at each amplifier site. The bandpass filter at the receiver part has a single-side pass bandwidth of $B_{pass} = 140\ GHz$.

Before the OTDM MUX, the data of *User2* is shifted by $3.5T_{FWHM}$ delay so that only the nearest solitons interact. Every user consists of 1024 bits with equal probability for '1' and '0'. Bit '1' of *User1*, or *User2*, is transmitted by sending a fundamental soliton of the form $P_0\text{sech}(t)$, or $r^2 P_0\text{sech}(rt)$ with $r = 1/\sqrt{2}$, and bit '0' is transmitted by sending nothing. The bit pattern at the various stages is shown in Fig 4.8.
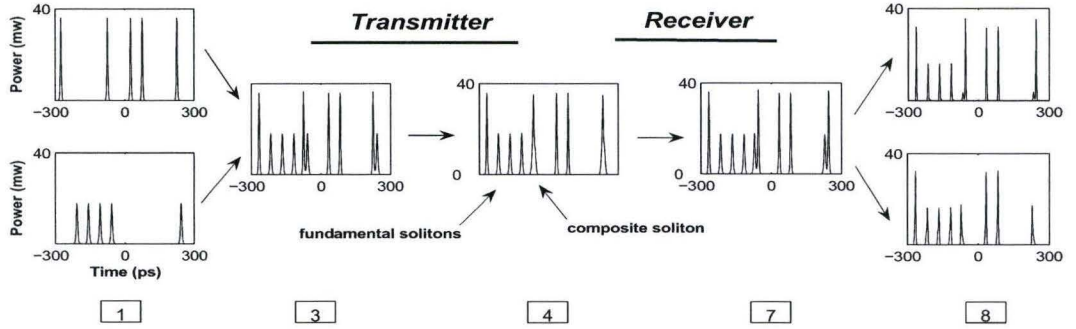
Figure 4.8: Modified signal flow chart through linear channels

Since bit '1' and bit '0' are equally likely to occur, therefore bits '11', '10', '01' and '00' are also equally distributed within the composite sequence. Then we obtain the TBP of the composite sequence such as

$$TBP_{Sequence} = \frac{1}{4}TBP_C + \frac{1}{2}TBP_F + \frac{1}{4} \times 0 = 0.4436 \tag{4.2}$$

Compared with the conventional TDM application using Gaussian pulses with bit rate $B = 40\ Gb/s$, whose TBP is 0.5, we can see that a saving of 11.29% in terms of TBP has been achieved here.

In the modified scheme, it is noted from both Fig 4.3 and Fig 4.8 that the lower fundamental soliton is ahead of the taller one at the initial point, while at the receiver part, it becomes reverse. However, since the two component solitons have *fixed* time shift, therefore fixed relative position to each other, it is not a problem to demultiplexing.

Fig 4.9 shows the eye-diagrams at the OTDM DEMUX (point 8 in Fig 4.8). It is noted that the inter-symbol interference (ISI) under this case is much heavier than that corresponding to the interaction between identical fundamental solitons. This is just because the non-linear interaction between different fundamental solitons is more unstable, and therefore more difficult to control. In the viewpoint of a single soliton-pair, we can increase the soliton DEMUX length to separate the component solitons more away from each other to decrease the ISI. However, it will cause heavier ISI between the adjacent time slot in a sequence.
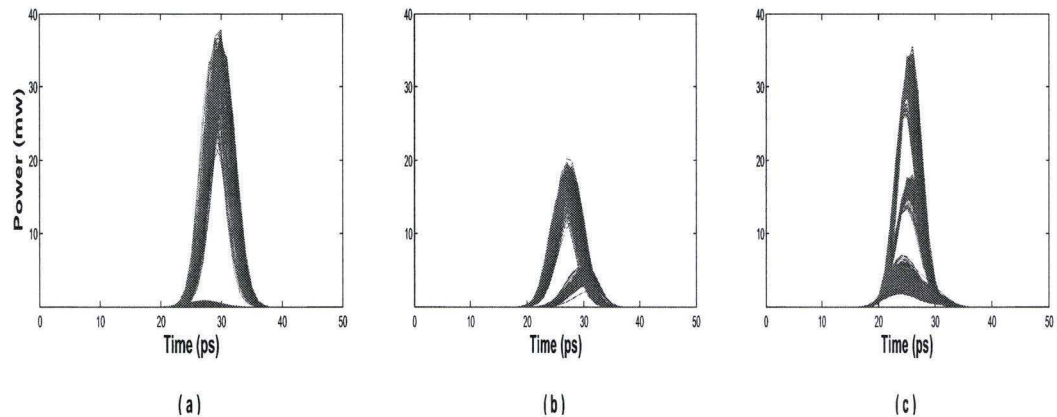
Figure 4.9: Eye-diagrams with $NF = 5.5 \ dB$. (a) *User1* demultiplexed from composite solitons, (b) *User2* demultiplexed from composite solitons, and (c) *User1* and *User2* demultiplexed from fundamental solitons.

4.4 Detection of Soliton Signals

4.4.1 General Approach

The problem of detecting a single soliton or multiple non-overlapping solitons in white Gaussian noise falls into the theory of classical detection. The general approach to such problems involves first mapping the observation waveform, $r(t)$ onto a convenient and

suitable compact decision space [26]. The detection problem then reduces to a partitioning of the decision space into decision regions according to a particular criteria of optimality. Consider the following binary hypothesis problem,

$$H_0 \quad : \quad r(t) = n(t)$$
$$H_1 \quad : \quad r(t) = s(t) + n(t)$$

where the received waveform comprises the soliton signals $s(t)$ in white Gaussian noise $n(t)$ under hypothesis '1', or just the noise $n(t)$ under the '0' hypothesis. The first task, reduction of $r(t)$ into a convenient decision space, is accomplished through the sufficient statistic,

$$z = \int r(t)s(t)dt \tag{4.3}$$

which can be efficiently computed with a matched filter.

Once the received signal has been transformed into the decision domain, we have the simple binary hypothesis test

$$H_0 \quad : \quad r = n$$
$$H_1 \quad : \quad r = s + n$$

where under $H_0 : r \sim \mathcal{N}(0, N)$, and under $H_1 : r \sim \mathcal{N}(P, N)$, where P and N are the soliton power and the noise power, respectively.

4.4.2 Bit Error Rate

For p-i-n receivers, the photocurrent is directly proportional to the incident power, such as

$$I = RP \tag{4.4}$$

where R is the responsivity of p-i-n receivers. For simplicity, R is chosen to be 1 here, and the p-i-n receiver is assumed to be noise free.

The performance criterion for digital receivers is governed by the *bit error rate* (BER), defined as the probability of incorrect identification of a bit by the decision circuit of the receiver part.

In a general case, the sampled value I fluctuates from bit to bit around an average value I_1 or I_0, depending on whether the bit corresponds to '1' or '0' in the sequence. The decision circuit compares the sampled value with a threshold value I_D and calls it bit '1' if $I > I_D$ or bit '0' if $I < I_D$. An error occurs if $I < I_D$ for bit '1' because of receiver noise and channel noise. A similar error also occurs if $I > I_D$ for bit '0'. Both sources of errors can be included by defining the BER as

$$\text{BER} = P(1)P(0|1) + P(0)P(1|0) \tag{4.5}$$

where $P(0)$ and $P(1)$ are the probabilities of receiving bits '0' or '1', respectively. $P(0|1)$ is the probability of deciding '0' when '1' is received, and $P(1|0)$ is the probability of deciding '1' when '0' is received. If '1' and '0' are equally likely to occur, $P(0) = P(1) = \frac{1}{2}$, and the BER becomes,

$$\text{BER} = \frac{1}{2}\left[P(0|1) + P(1|0)\right] \tag{4.6}$$

Both $P(0|1)$ and $P(1|0)$ depend on the probability density function $P(I)$ of the sampled value I. The functional form of $P(I)$ depends on the statistics of noise sources responsible for current fluctuations. Suppose the noise source can be described by the additive white Gaussian noise (AWGN) statistics with zero mean, then the sampled value I also has a Gaussian probability density function. Both the average and the variance are different for bits '1' and '0' since I equals I_1 or I_0, depending on the bit received. If σ_1^2 and σ_0^2 are the corresponding variances, the conditional probabilities are given by

$$P(0|1) = \frac{1}{\sqrt{2\pi}\sigma_1} \int_{-\infty}^{I_D} \exp\left[-\frac{(I - I_1)^2}{2\sigma_1^2}\right] dI = \frac{1}{2}\text{erfc}\left(\frac{I_1 - I_D}{\sqrt{2}\sigma_1}\right) \tag{4.7a}$$

$$P(1|0) = \frac{1}{\sqrt{2\pi}\sigma_0} \int_{I_D}^{\infty} \exp\left[-\frac{(I - I_0)^2}{2\sigma_0^2}\right] dI = \frac{1}{2}\text{erfc}\left(\frac{I_D - I_0}{\sqrt{2}\sigma_0}\right) \tag{4.7b}$$

where $erfc(\cdot)$ stands for the complementary error function, defined as

$$\text{erfc}(x) = \frac{2}{\sqrt{\pi}} \int_x^{\infty} \exp(-y^2)dy \tag{4.8}$$

By substituting Eq.(4.7) into Eq.(4.6), the BER is given by

$$BER = \frac{1}{4}\left[\text{erfc}\left(\frac{I_1 - I_D}{\sqrt{2}\sigma_1}\right) + \text{erfc}\left(\frac{I_D - I_0}{\sqrt{2}\sigma_0}\right)\right] \qquad (4.9)$$

Eq.(4.9) shows that the BER depends on I_D. In practice, when $\sigma_1 = \sigma_0$, I_D is usually optimized as the middle value of I_1 and I_0 to minimize the BER.

4.4.3 Detection Algorithm

For convenience, we replot the eye-diagrams in Fig 4.9 again in the noise-free environment within one figure, as shown in Fig 4.10.
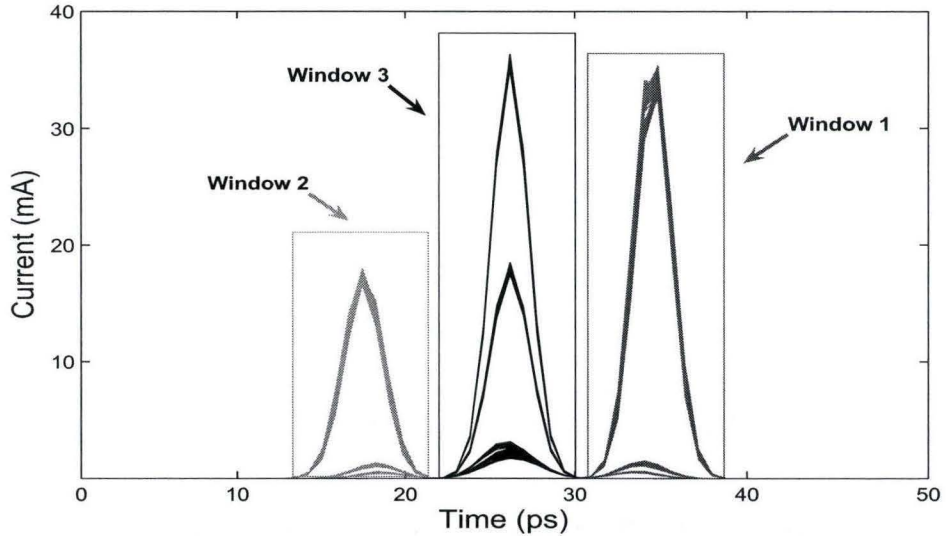
Figure 4.10: Detection windows for different received signals.

As we have mentioned above, there are together four kinds of composite pulses transmitted within this scheme, i.e., '00', '11', '01', and '10'.

- For '00', we send nothing for this composite pulse.

- For '11', we send $P_0\text{sech}(t)$ and $r^2 P_0\text{sech}(rt)$, respectively, for *User1* and *User2*. According to the simulation results from Fig 4.2, we can adjust the soliton DEMUX

38

length to let the two component solitons deviate from each other with any separation space, $0 \to \infty$. Considering the interference between time slots, here we select the point where the two component solitons are demultiplexed with the same separation as that at the transmitter part.

It is noted that in the transmitter part, *User2* is ahead of *User1*, however, they are reversed at the receiver part. That is, *User1*, which has a higher power level, is ahead of *User2*. Since both component solitons have *fixed* time shift, it is not a problem to demultiplex.

- For '10' or '01', these two kinds of pulses are in fact only two kinds of fundamental solitons accounting for *User1* and *User2*, respectively. Therefore, they are pure fundamental solitons and reach the receiver part without distortion in ideal conditions.

As shown in Fig 4.10, there are together 3 parts in the received signals. The parts in window 1 and window 2 are both demultiplexed from the composite solitons, which are dependent on each other. That is, if there is a pulse '1' in window 1, then there muse be a corresponding pulse '1' in window 3, since they both come from the same single composite soliton. The part in window 3 is demultiplexed from the fundamental solitons, which includes pulses from both *User1* and *User2*.

Since there are 3 types of center points, a two-step Electro-Absorption Modulator (EAM) is used at the receive part. The detailed detection algorithm is listed as follows.

Step 1 : Use window 1 and window 2 to detect the solitons having been transmitted in the form of composite solitons, i.e., detecting '**11**'. Since their relative positions are known *a priori*, then the detection problem reduces to two parallel standard Gaussian detection problems,

for window 1

$$
\begin{aligned}
H_0 &: \quad r(t) = n(t) & \text{no user is present,} \\
H_1 &: \quad r(t) = s_1(t) + n(t) & \textit{User1} \text{ is present}
\end{aligned}
$$

The sampled value I fluctuates around an average value I_{11} for bit '1', or I_{10} for bit '0' in the sequence, where the first '1's in the subscripts represent window 1, while the second '1', or '0', represents bit '1', or bit '0'. Especially in window 3, the second '1', or '2', represents the lower-energy soliton, or the higher-energy soliton, which will be discussed later. The decision part compares the sampled value with a threshold value I_{D1} and decides it as '1' if $I > I_{D1}$, or as '0' if $I < I_{D1}$.

for window 2

$$H_0 \quad : \quad r(t) = n(t) \qquad\qquad \text{no user is present,}$$

$$H_2 \quad : \quad r(t) = s_2(t) + n(t) \qquad \textit{User2} \text{ is present.}$$

Similarly, the decision part compares the sampled value, I, with a threshold value I_{D2} and decides it as '1' if $I > I_{D2}$, or as '0' if $I < I_{D2}$.

Both of the above detection problems can be solved with the standard two-level Gaussian detection theory.

It is noted that here bit '1' in *User1* and bit '1' in *User2* are in coupled form. That is, when we detect H_1 in window 1, it must be H_2 in window 2 in theory. Therefore, in a simplified architecture, we can only set window 1, for its higher signal power is more likely correctly detected, in the detection procedure.

Step 2 : Using window 3 to detect the solitons having been transmitted in the form of fundamental solitons, i.e., '**10**' or '**01**'. Since their relative positions are also known *a priori* and the powers used for *User1* and *User2* are different, then the detection problem reduces to a standard multi-level Gaussian detection process,

for window 3

$$H_0 \quad : \quad r(t) = n(t) \qquad\qquad \text{no user is present,}$$

$$H_1 \quad : \quad r(t) = s_1(t) + n(t) \qquad \textit{User1} \text{ is present,}$$

$$H_2 \quad : \quad r(t) = s_2(t) + n(t) \qquad \textit{User2} \text{ is present.}$$

Straightforwardly, if we detect H_1, then a decision of '**10**' can be made. Similarly, H_2 is corresponding to '**01**'. Finally, if H_0, also considering the result from *step 1*, we can say the received bits are '**00**'.

4.4.4   Simulation Result Analysis

Since the window 2 can be ignored for simplicity, Fig 4.11 only shows the eye-diagrams of the demultiplexed pulses in window 1 and window 3, respectively, at the receiver part, where I_{11}, I_{10}, and I_{32}, I_{31}, I_{30} represent the average signal powers at the sample points, while I_{D1}, I_{D31} and I_{D32} are the corresponding decision thresholds.
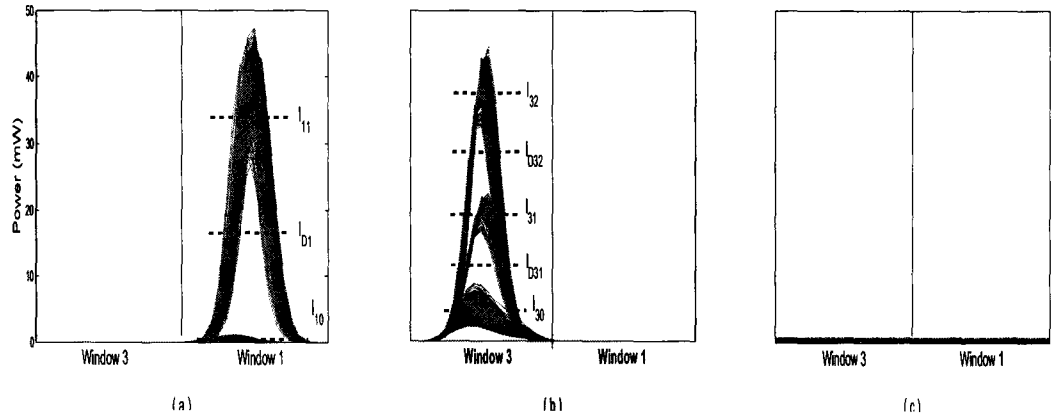
Figure 4.11: Detection Scheme at the receiver part. (a) Combination of '11', (b) Combination of '10' (larger amplitudes) and '01' (small amplitudes), and (c) Combination of '00'.

In our scheme, we extend the definition of BER in the previous part, and the combination of '00', '01', '10' or '11' is taken as a single couple. For example, in the case of '00', if we receive '11', '10' or '01', an error happens. Therefore, the BER in our scheme can be given as

$$P_e = P_{e00} + P_{e01} + P_{e10} + P_{e11} \qquad (4.10)$$

41

where

$$
\begin{aligned}
P_{e00} &= P(00)\left[P(11|00) + P(10|00) + P(01|00)\right] \\
P_{e01} &= P(01)\left[P(11|01) + P(10|01) + P(00|01)\right] \\
P_{e10} &= P(10)\left[P(11|10) + P(01|10) + P(00|10)\right] \\
P_{e11} &= P(11)\left[P(10|11) + P(01|11) + P(00|11)\right].
\end{aligned}
$$

For P_{e00}, we have

$$
P(01|00) = \frac{1}{\sqrt{2\pi}\sigma_{30}} \int_{I_{D32}}^{I_{D31}} \exp\left[-\frac{(I-I_{30})^2}{2\sigma_{30}^2}\right] dI \cdot \frac{1}{\sqrt{2\pi}\sigma_{10}} \int_{0}^{I_{D1}} \exp\left[-\frac{(I-I_{10})^2}{2\sigma_{10}^2}\right] dI
$$

$$
P(10|00) = \frac{1}{\sqrt{2\pi}\sigma_{30}} \int_{I_{D31}}^{\infty} \exp\left[-\frac{(I-I_{30})^2}{2\sigma_{30}^2}\right] dI \cdot \frac{1}{\sqrt{2\pi}\sigma_{10}} \int_{0}^{I_{D1}} \exp\left[-\frac{(I-I_{10})^2}{2\sigma_{10}^2}\right] dI
$$

$$
P(11|00) = \frac{1}{\sqrt{2\pi}\sigma_{30}} \int_{0}^{I_{D32}} \exp\left[-\frac{(I-I_{30})^2}{2\sigma_{30}^2}\right] dI \cdot \frac{1}{\sqrt{2\pi}\sigma_{10}} \int_{I_{D1}}^{\infty} \exp\left[-\frac{(I-I_{10})^2}{2\sigma_{10}^2}\right] dI.
$$

For P_{e01}, we have

$$
P(00|01) = \frac{1}{\sqrt{2\pi}\sigma_{32}} \int_{I_0}^{I_{D32}} \exp\left[-\frac{(I-I_{32})^2}{2\sigma_{32}^2}\right] dI \cdot \frac{1}{\sqrt{2\pi}\sigma_{10}} \int_{0}^{I_{D1}} \exp\left[-\frac{(I-I_{10})^2}{2\sigma_{10}^2}\right] dI
$$

$$
P(10|01) = \frac{1}{\sqrt{2\pi}\sigma_{32}} \int_{I_{D31}}^{\infty} \exp\left[-\frac{(I-I_{32})^2}{2\sigma_{32}^2}\right] dI \cdot \frac{1}{\sqrt{2\pi}\sigma_{10}} \int_{0}^{I_{D1}} \exp\left[-\frac{(I-I_{10})^2}{2\sigma_{10}^2}\right] dI
$$

$$
P(11|01) = \frac{1}{\sqrt{2\pi}\sigma_{32}} \int_{0}^{I_{D32}} \exp\left[-\frac{(I-I_{32})^2}{2\sigma_{32}^2}\right] dI \cdot \frac{1}{\sqrt{2\pi}\sigma_{10}} \int_{I_{D1}}^{\infty} \exp\left[-\frac{(I-I_{10})^2}{2\sigma_{10}^2}\right] dI.
$$

For P_{e10}, we have

$$
P(01|10) = \frac{1}{\sqrt{2\pi}\sigma_{31}} \int_{I_{D32}}^{I_{D31}} \exp\left[-\frac{(I-I_{31})^2}{2\sigma_{31}^2}\right] dI \cdot \frac{1}{\sqrt{2\pi}\sigma_{10}} \int_{0}^{I_{D1}} \exp\left[-\frac{(I-I_{10})^2}{2\sigma_{10}^2}\right] dI
$$

$$
P(00|10) = \frac{1}{\sqrt{2\pi}\sigma_{31}} \int_{0}^{I_{D32}} \exp\left[-\frac{(I-I_{31})^2}{2\sigma_{31}^2}\right] dI \cdot \frac{1}{\sqrt{2\pi}\sigma_{10}} \int_{0}^{I_{D1}} \exp\left[-\frac{(I-I_{10})^2}{2\sigma_{10}^2}\right] dI
$$

$$
P(11|10) = \frac{1}{\sqrt{2\pi}\sigma_{31}} \int_{0}^{I_{D32}} \exp\left[-\frac{(I-I_{31})^2}{2\sigma_{31}^2}\right] dI \cdot \frac{1}{\sqrt{2\pi}\sigma_{10}} \int_{I_{D1}}^{\infty} \exp\left[-\frac{(I-I_{10})^2}{2\sigma_{10}^2}\right] dI.
$$

For P_{e11}, we have

$$
P(01|11) = \frac{1}{\sqrt{2\pi}\sigma_{30}} \int_{I_{D32}}^{I_{D31}} \exp\left[-\frac{(I-I_{30})^2}{2\sigma_{30}^2}\right] dI \cdot \frac{1}{\sqrt{2\pi}\sigma_{11}} \int_{0}^{I_{D1}} \exp\left[-\frac{(I-I_{11})^2}{2\sigma_{11}^2}\right] dI
$$

$$
P(10|11) = \frac{1}{\sqrt{2\pi}\sigma_{30}} \int_{I_{D31}}^{\infty} \exp\left[-\frac{(I-I_{30})^2}{2\sigma_{30}^2}\right] dI \cdot \frac{1}{\sqrt{2\pi}\sigma_{11}} \int_{0}^{I_{D1}} \exp\left[-\frac{(I-I_{11})^2}{2\sigma_{11}^2}\right] dI
$$

$$
P(00|11) = \frac{1}{\sqrt{2\pi}\sigma_{30}} \int_{0}^{I_{D32}} \exp\left[-\frac{(I-I_{30})^2}{2\sigma_{30}^2}\right] dI \cdot \frac{1}{\sqrt{2\pi}\sigma_{11}} \int_{0}^{I_{D1}} \exp\left[-\frac{(I-I_{11})^2}{2\sigma_{11}^2}\right] dI.
$$

In our modified soliton multiplexing scheme, we confine both the soliton multiplexing scheme and the conventional TDM scheme of the same frequency bandwidth in terms of the root mean square (RMS) width, here 29.45 GHz. Considering the channel spacing in practice, we multiplex 6 users within one time slot. Since the soliton multiplexing scheme has a less TBP, i.e., a less temporal width in this case, it possesses a less crosstalk interference compared with the conventional TDM scheme, and therefore, a lower BER. Specially, for the typical in-line amplifier number of 5 for a 400 km transmission, our BER is about 3.7 dB lower.
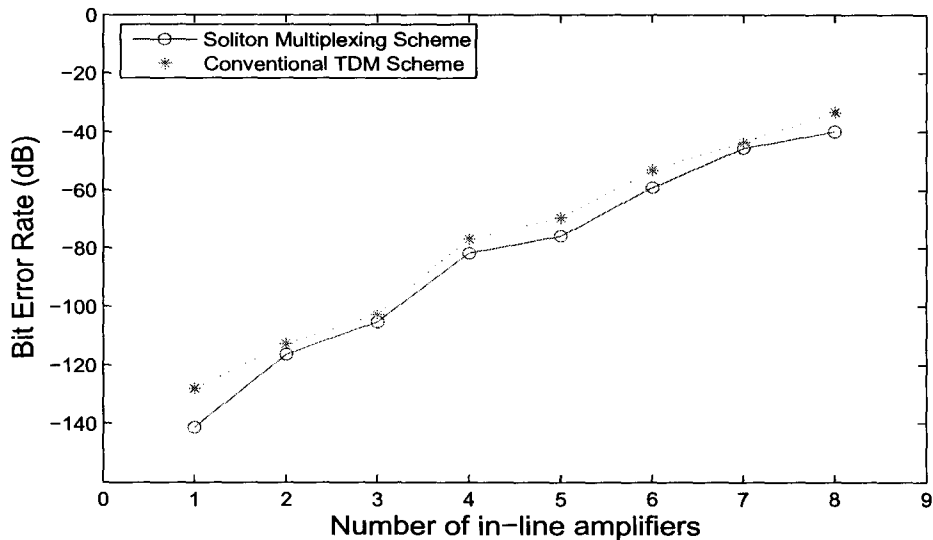

Figure 4.12: Scheme BER under different number of in-line amplifiers

Chapter 5

Conclusions and Directions for Future Work

5.1 Conclusions

In the thesis, we have developed a framework for exploring the processing of soliton signals and introduced an application of solitons in the broad context of optical communications.

We have taken the viewpoint of using optical solitons as carrier signals for transmission over both linear and quasi-linear channels. The NSE is viewed as the specialized processor of this kind of signals, which are naturally suited to performing a number of complex signal processing tasks. For example, this system can efficiently perform the nonlinear signal combination and separation of multi-soliton carriers necessary for multiplexing and demultiplexing multiple users in a potential free space or fiber-based optical communications context.

Focusing specially on the optical TDM scheme using soliton interaction, we develop a new optical realization form for the processing of optical soliton signals. Although analog circuit models have been previously developed for a variety of nonlinear wave equations in general, and for the Toda lattice in particular [1, 2], our optical TDM scheme is a good direct optical analog of this kind of soliton system. Further, this appears to be a good optical model of the NSE which is sufficiently accurate to demonstrate the soliton interaction.

The optical TDM model using soliton interaction is used to multiplex multiple signals onto a multi-soliton carrier. We have demonstrated that the nonlinear interaction of multiple solitons can be explored as a means of saving the signals' time-bandwidth product (TBP) in a multi-user communication context.

5.2 Future Directions

In the thesis, we began an exploration of a new and interesting application of soliton signals and systems from a signal processing viewpoint. As a result, there are a number of outstanding issues relating to the topics considered. Here, we just mention several particularly intriguing directions.

Much of the mathematical foundation for soliton dynamics lies within the framework of solvable nonlinear systems. In Chap.3 and Chap.4, we illustrate how the schemes can be used in the context of optical communications. These results illustrate the potential for development of a variety of hardware for soliton modulation techniques. However, there are several outstanding issues regarding the detailed implementation of the communications techniques discussed in Chap.4. Specifically, the demodulation of individual soliton carriers still must be addressed with a more complete investigation into the effects of channel nonlinearity and realistic non-additive channel disturbances. From the viewpoint of system design, these two points will lead to jitter in the arrival time of solitons because the phase of composite solitons is not likely to remain well controlled.

Although we have explored some basic strategies for using soliton interaction in optical communications, there remain a number of unanswered questions regarding the efficacy of such techniques in comparison to standard methods. For example, the complexity of the electrical pre-process device for such methods in comparison to standard techniques ought to be undertaken. Finally, we note that solitons represent a rich class of signals that are potentially applicable to a variety of signal processing and communications contexts beyond those mentioned in the thesis. Indeed, perhaps the most exciting and potentially rewarding direction for future research lies in the discovery of new and promising applications.

Bibliography

[1] A. C. Singer, A. V. Oppenheim and G. W. Wornell, "Detection and Estimation of Multiplexed Soliton Signals", IEEE Trans. Signal Processing, vol.**47**, pp. 2768-2782, 1999.

[2] R. Chai and K. M. Wong, "Application of Solitons in Multiplexing", Proc. IWDDC, Edinburgh, UK, 2004.

[3] G. P. Agrawal, Nonlinear Fiber Optics, Second Edition, Academic, 1995.

[4] A. Hasegawa, Optical Solitons in Fibers, Second Edition, Springer, 1989.

[5] A. Hasegawa, "Soliton-Based Optical Communications: An Overview", IEEE J. Quantum Electronics, vol.**6**, pp. 1161-1172, 2000.

[6] C. S. Gardner, J. M. Greene, M. D. Kruskal, and R. M. Miura, "Method for solving the Korteweg-de Vries equation", Phys. Rev. Lett., vol.**19**, pp. 1095-1097, 1967.

[7] M. A. Ablowitz, and P. A. Clarkson, Solitons, Nonlinear Evolution Equations and Inverse Scattering, Cambridge University Press, 1991.

[8] M. Du, A. K. Chan, and C. K. Chui, "A novel approach to solving the nonlinear Schrodinger equation by the coupled amplitude-phase formulation", IEEE J. Quantum Electronics, vol.**31**, pp. 177-182, 1995.

[9] H. Ghafouri-Shiraz, P. Shum, and M. Nagata, "A novel method for analysis of soliton propagation in optical fibers", IEEE J. Quantum Electronics, vol.31, pp. 190-200, 1995.

[10] D. Anderson, and M. Lisak, "Bandwidth limits due to mutual pulse interaction in optical soliton communication systems", Optics Letters, vol.11, No.3, pp. 174-176, 1986.

[11] S. Dolinar, D. Divsalar, J. Hamkins, and F. Pollara, "Capacity of Pulse-Position Modulation (PPM) on Gaussian and Webb Channels", TMO Progress Report, pp. 42-142, 2000.

[12] M. Nakazawa, K. Suzuki, H. Kubota, E. Yamada, and Y. Kimura, "Dynamic optical soliton communication", IEEE J. Quantum Electronics, vol.26, pp. 2095-2102, 1990.

[13] V. N. Serkin, and A. Hasegawa, "Exactly integrable nonlinear Schrodinger equation models with varying dispersion, nonlinearity and gain application for soliton dispersion", IEEE J. Quantum Electronics, vol.8, pp. 418-431, 2002.

[14] F. M. Mitschke, and L. F. Mollenauer, "Experimental observation of interaction forces between solitons in optical fibers", Optics Letters, vol.12, No.5, pp. 355-357, 1987.

[15] D. Schrader, "Explicit calculation of N-soliton solutions of the nonlinear Schroedinger equation", IEEE J. Quantum Electronics, vol.31, pp. 2221-2225, 1995.

[16] H. Toda, K. Mino, Y. Kodama, A. Hasegawa, and P. A. Andrekson, "Influence of noise in optical pulse source on soliton transmission", J. Lightwave Technology, vol.17, No.6, pp. 1027-1031, 1999.

[17] J. P. Gordon, "Interaction forces among solitons in optical fibers", Optics Letters, vol.8, No.11, pp. 596-598, 1983.

[18] M. Nakazawa, and H. Kubota, "Optical soliton communication in a positively and negatively dispersion-allocated optical fiber", Electronics Letters, vol.**31**, No.**3**, pp. 216-217, 1995.

[19] Y. Kodama, and K. Nozaki, "Soliton interaction in optical fibers", Optics Letters, vol.**12**, No.**12**, pp. 1038-1040, 1987.

[20] C. Desem, and P. L. Chu, "Soliton interaction in the presence of loss and periodic amplification in optical fibers", Optics Letters, vol.**12**, No.**5**, pp. 349-351, 1987.

[21] N. J. Doran, and K. J. Blow, "Solitons in optical communications", IEEE J. Quantum Electronics, vol.**QE-19**, pp. 1883-1888, 1983.

[22] L. D. Carr, C. W. Clark, and W. P. Reinhardt, "Expected and Unexpected Solutions to the Stationary One-Dimensional Nonlinear Schrödinger Equation", World Scientific, 1999.

[23] S. Kumar, and A. Hasegawa, "Suppression of the Gordon-Haus noise", Optics Letters, vol.**20**, No.**18**, pp. 1856-1858, 1995.

[24] J. R. Taylor, Optical Solitons – Theory and Experiment, Cambridge Univesity, 1992.

[25] D. Slepian, "Some comments on Fourier analysis, uncertainty and modelling", SIAM Review, vol.**25**, No.**3**, pp. 379-393.

[26] H. L. Van Trees, "Detection, Estimation, and Modulation Theory: Part I Detection, Estimation, and Linear Modulation Theory", John Wiley and Sons, 1968.

[27] C. W. Helstrom, "Statistical Theory of Signal Detection", Pergamon Press, New York, Second Edition, 1968.

[28] S. Bloom, J. Schuster, and H. A. Willebrand, "Understanding the Performance of Free-Space Optics", WCA Technical Symposium, San Jose, 2003.

[29] R. Hirota, The Direct Method in Soliton Theory, Cambridge University Press, 2004.

[30] G. L. Lamb, Elements of Soliton Theory, Wiley, 1980.

[31] A. S. Fokas, and V. E. Zakharov, Important Developments in Soliton Theory, Springer, 1993.

[32] D. H. Sattinger, C. A. Tracy, and S. Venakides, Inverse Scattering and Applications, American Mathematical Society, 1991.

[33] I. Kay, and H. E. Moses, Inverse Scattering Papers 1955-1962, Math Sci Press, 1982.

[34] H. P. Baltes, Inverse Scattering Problems in Optics, Springer-Verlag, 1980.

[35] W. Eckaus, and A. Van Harten, The Inverse Scattering Transformation and the Theory of Solitons: An Introduction, North-Holland, 1981.

[36] M. Toda, Nonlinear Waves and Solitons, Kluwer Academic Publishers, 1989.

[37] E. Infeld, and G. Rowlands, Nonlinear Waves, Solitons, and Chaos, Cambridge University Press, 2000.

[38] A. Hasegawa, and M. Matsumoto, Optical Solitons in Fibers, Springer, 2003.

[39] R. K. Dodd, Solitons and Nonlinear Wave Equations, Academic Press, 1984.

[40] C. Rebbi, and G. Soliani, Solitons and Particles, World Scientific, 1984.

[41] S. Novikov, Theory of Solitons: the Inverse Scattering Methods, Consultants Bureau, 1984.

[42] M. Remoissenet, Waves Called Solitons: Concepts and Experiments, Springer-Verlag, 1994.